


ITC 1/49 Information Technology and Control Vol. 49 / No. 1 / 2020 pp. 55-79 DOI/10.5755/j01.itc.49.1.24140	Hand Contour Classification Using Differential Evolution Algorithm with Ensemble of Parameters and Mutation and Crossover	
	Received 2019/09/04	Accepted after revision 2019/11/19
	 http://dx.doi.org//10.5755/j01.itc.49.1.24140	

HOW TO CITE: Moravec, J. (2020). Hand Contour Classification Using Differential Evolution Algorithm with Ensemble of Parameters and Mutation and Crossover. *Information Technology and Control*, 49(1), 55-79. <https://doi.org//10.5755/j01.itc.49.1.24140>

Hand Contour Classification Using Differential Evolution Algorithm with Ensemble of Parameters and Mutation and Crossover

J. Moravec

Faculty of Electrical Engineering and Informatics; University of Pardubice; náměstí Čs. legií 565, 530 02 Pardubice, Czech Republic; phone: +420 466 036 11

Corresponding author: jaroslav.moravec@student.upce.cz (j.moravec.email@seznam.cz)

Biometrical identification of persons using the contour of a human hand belongs to a very interesting and not yet totally explored areas, and its accuracy and effectiveness depends, to some extent, on the technical possibilities in scanning of persons. The presented paper solves the problem with use of a combination of various methods. A hand contour, topological description of the hand, evolutionary algorithm, and linear regression algorithm to estimate correct knuckles positions is used. For comparison of geometrical data, the Iterative Closest Point (ICP) algorithm is used in its genuine shape. Just the modern evolutionary optimizers enabling to change from ground the view how to solve similar problems but at the expense of higher algorithm development demands. However, it enables to cut down computational demands of ICP algorithm markedly. Experimental verification of proposed methods was performed with use of two different databases THID and GPDS with persons of different gender and age (c. 20-65 years) with total number of persons in individual databases 104 and 94. Experimental results proved very successfully the suitability of use the combination of the methods ICP and evolutionary optimizer called EPSDE for solving the given task with final algorithmic complexity $O(N)$ and successful rate at classification given by coefficients THID:EER=0.38% and GPDS:EER=0.35% on real images.

KEYWORDS: Biometric identification, contour classification, evolutionary algorithm, linear regression.

1. Introduction

The Persons identification problem with use of hand contour [8, 7, 14, 29, 33, 50] is very specific. It is a de-facto accurate measurement of dynamically changeable two-dimensional structures based only on visual information. A successful solution of this problem requires use of high-quality apparatus to obtain images of hands, sophisticated hand image processing and computing of hand contour, and of course high-quality filtering of noise. The problem of hand contour classification is then defined as the capability of classifier to find, as near as possible, the correspondence between template hand contour, and contour which is submitted for identification. All five fingers of the template contour of a hand are moveable, and thanks to that the classification process is more difficult compared with a hand contour which has only four fingers. The big challenges which depend purely on technical advance is firstly, image filtration received from common mobile equipment and secondly, finding correct positions of individual knuckles. This is because it is not possible to repeatedly use x-ray or magnetic resonance for person identification as it is very expensive. In the survey study [8] a list of best possible results is mentioned which can be reached with use of a certain type of algorithm. The methods based on simple Euclidean metrics can reach accuracy defined by a coefficient approx. EER=3-5%. This fact is commonly known.

A method described in the presented paper modifies, in a suitable way, a commonly used scheme of Euclidean metrics. It uses a modern, and many years proved, evolutionary optimizer of 3rd generation and an Iterative Closest Point (ICP) algorithm [10]. Thanks to this combination the method is capable of coming up with results of methods which are based on the Linear Discriminant Analysis (LDA) algorithm, which is at this time assumed as one of the best possible solutions for the given task and which is used in many papers e.g. in [8, 35]. An advantage of the proposed method is also lower algorithmic complexity in comparison to LDA vs ICP+EA however, at the expense of higher algorithmic demands (code length). Biometric identification of persons with use of hand contour falls into the category of methods of short-term identification, and very often works in connection with any other biometric method. Biometrical information of a human has one undisputable advantage. It is difficult to forget it and even worse it can be falsified if a tested person is physically present. During personal identi-

fication, more features are combined very often e.g. hand contour and palmprint, finger print, palmprint only, skin folds on fingers, hand bloodstream, iris, ear shape, and face shape. Moreover, it is possible to take into account the classic PIN code. As an example, personal identification in airports with use of ear photos can be mentioned [1, 28].

For experimental purposes two different databases were used: Technocampus hand Image Database (THID) [20, 23, 58] and also database GPDS [22, 55, 59] The Grupo de Procesado Digital de la señal, GPDS (Digital Signal Processing Group) with DPDS (División de Procesado Digital de la Señal) from Instituto para el Desarrollo Tecnológico y la Innovación en Comunicaciones IDeTIC, University of Las Palmas de Gran Canaria, Spain.

2. Related Works

2.1. Selected Methods of Persons Identification with Use of Hand Contour Representation

There is an uncountable number of methods based on biometrics published in the past, and new methods still arise. However, the area of person identification with use of hand contour classification is not so wide and publications are rarer. [19, 20] presented an algorithm enabling personal identification with use of hand contour and neural nets of Multi-Layer Perceptron (MLP) type. Success rate of the method is in the 99-100 percent interval. Another use of neural nets can be found e.g. in [3]. [8] published a paper based on their own many years of long research. They also used findings of other research teams e.g. [13, 50]. The best results were reached with use of the Linear Discriminant Analysis (LDA) algorithm and the final coefficient is EER=0.52%. The value of EER=3.5% was obtained when using the standardized Euclidean distance algorithm. [5] published a method called the "multimodal biometric system", which for identification of persons, uses hand contour and also other geometric primitives. The best reached result is EER=0.31% with use of images from a proprietary database, and EER=0.52% with use of images from IITD database. [33] proposed

a method called “Hand Geometry and Crookedness Identification Algorithm” (HG CIA). The best reached accuracy is for a template made of three hand images FAR=0.0%, FRR=1.19%, IR=100% in identification mode and FAR=0.03%, FRR=1.19% in verification mode. Without use of weight coefficients they reached a fantastic FAR=1.19%, FRR=1.19%. [35] proposed a method named GA-LDA, which utilizes a Genetic Algorithm (GA) in combination with the Linear Discriminant Analysis (LDA). GA is not used for classification of contours but only in the preprocessing step. The method that provided the best results with accuracy of 100 percent for the GPDS database had a subset of 22 and 34 significant features. The result for the IITD database was EER=4.6%. [9] proposed a method which enables classification of a hand contour with the use of a “k-nearest neighbours” (kNN) classifier, which was obtained from [35]. These authors also used a classifier called “Random Forest”. Both classifiers work with a set of features instead of a two-dimensional shape of hand contour. The best reached value of EER when only using 4 fingers is EER=6.6-8.0% for the right hand and EER=6.2-8.25% for the left hand according to the number of persons in the used database. With an increasing number of persons, the accuracy decreases.

2.2. Algorithm ICP

For comparison purposes of two hand contours the algorithm named Iterative Closest Point (ICP) was elected [10]. ICP is somewhat older, but still much-used algorithm. There is an uncountable number of modifications. The ICP algorithm represents many years of proved technology which because of its benefits, is more often used in sensitive areas of medicine e.g. [19]. Convergence analysis of the ICP algorithm is mentioned in [10, 43, 36] and other useful information can be found in [46].

2.3. Elected Evolutionary Optimizers

For computation purposes of personal identification with use of hand contour, the EPSDE algorithm [37] is primarily used, which originates from optimizer Differential Evolution (DE) [44], algorithm jDE [11] and algorithm JADE [61]. The reason why the EPSDE algorithm was elected is that at experiments, it showed the best results. EPSDE totally minimizes the number of working parameters see [17, 51, 52, 53]. In the experimental results section, several other optimizers: SaDE [45], SPDE [2], DESAP [54], SANSDE [62],

CMA-ES [24, 25, 26], Particle Swarm Optimization (PSO) [32], RPSO [57] and SGA [27, 28], Polar Bear Optimizer (PBO) [42] are also used. All used optimizers optimize 7, 8 and 9-dimensional functions which are constrained, noncontinuous, non-separable, strongly nonlinear and ill conditioned. As the most suitable optimizer from the set of tested optimizers, EPSDE was elected. Now, several important notations will be described which relate to the EPSDE optimizer and are used in the following paragraphs.

For evolutionary optimizers, the first step of the algorithm is usually initialization of the population P_{op} of individuals in the total number of N_{pop} individuals $X_i | i \in \langle 0, N_{pop} \rangle, N_{pop} \in \mathbb{N}^+, N_{pop} \geq 4, X_i = [x_j | j \in \langle 0, D_{im} \rangle, F | j \in \langle 0.0, 2.0 \rangle], x_j \in \mathbb{R}$. Every individual X_i represents one possible solution of the given task. X_i is a D_{im} -dimensional vector which brings concrete values (real numbers) for one possible solution in actual generation G_{en} . Parameter F is marked as a mutational (weight) constant and holds that $0.0 < F \leq 2.0$. EPSDE computes F automatically. In the first step of the algorithm all individuals are placed to random position in whole space of possible solutions $H = D_{om}^1 \times D_{om}^2 \times \dots \times D_{om}^k | k \in \mathbb{N}^+, D_{om}$ is so called domain for k th dimension, $D_{om} | D_{om} \in (\min, \max)$, every dimension can have different values **min**, **max** resp. limitations of space of possible solutions.

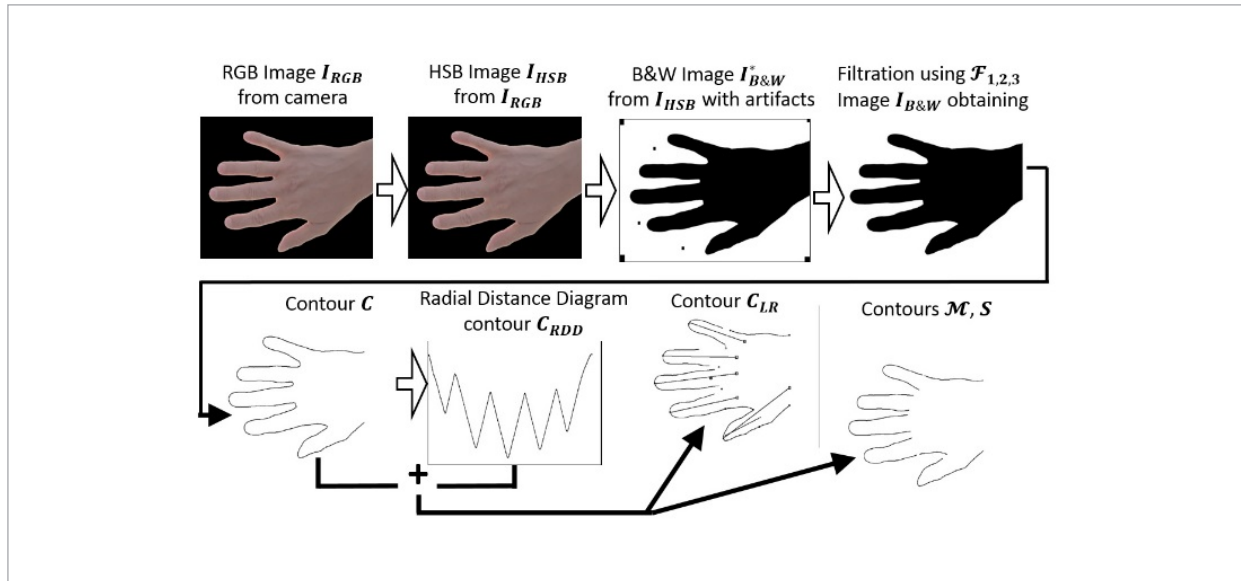
After initialization follows an iterative process of evolution which is usually given with number of generations G_{en} and at the end of this process the optimizer provides a result.

3. Description of Proposed Method

The presented system for personal identification using contour of a human hand belongs to the group of contactless systems. The proposed algorithm will be marked as **eaICP**. It is not necessary that a hand touches a pad during image capturing, but it is possible. The algorithm cannot work with scale, hence, it is assumed that movement in the Y axis is minimal, or it must be limited with suitable means e.g. glass desks. The hand is inserted into a sensing chamber or sensing area in a defined direction and angle, with the top of the hand heading to the camera and with stretched fingers. The angle between the hand axis and the X axis must be as small as possible – see Fig. 1 and 3.

Figure 1

Gradual process of image processing from camera – see also Figures 1-2. Firstly, an image from camera is captured, then image transformation follows into suitable format, next is conversion to black and white representation and next is image filtration and analytical description creation and creation of contours suitable for computation with EA and ICP

**Figure 2**

Scheme of process of classification of found contour of hand C – see also (3). The contour C is classified with use of Radial Distance Diagram R_{DD} see (2) and significant points P_C (points of inflexion of the curve). By this step a curve C_{RDD} is obtained see (3). With use of contour C and found significant points P_C on curve R_{DD} resp. C_{RDD} , axes of individual fingers are then found with use of contour C_{LR} and next the contours M and S are assembled

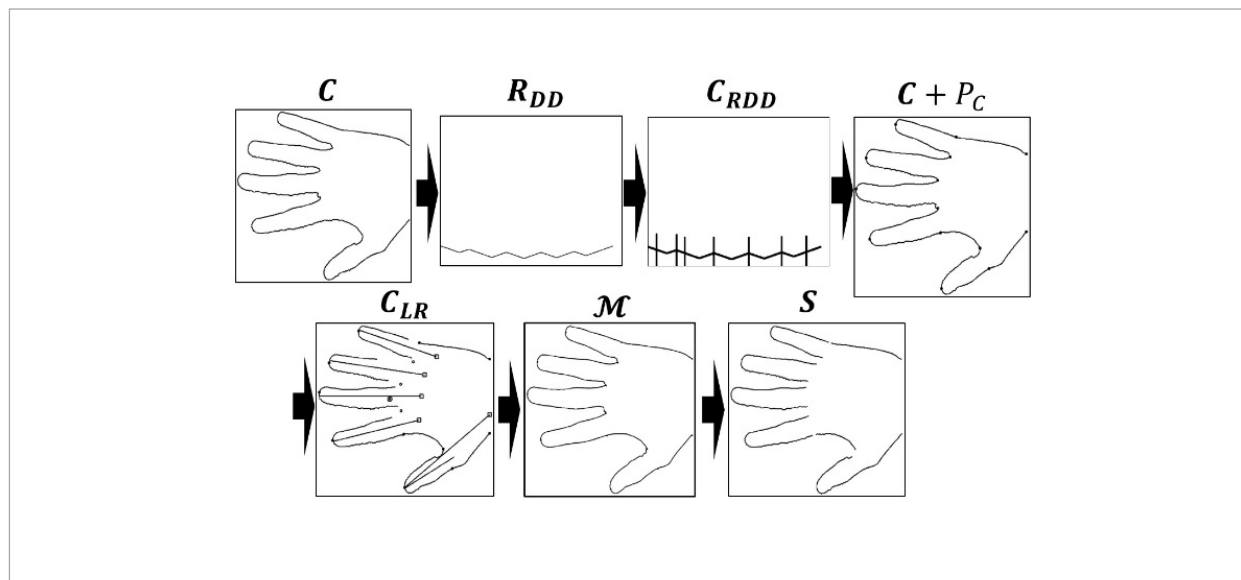
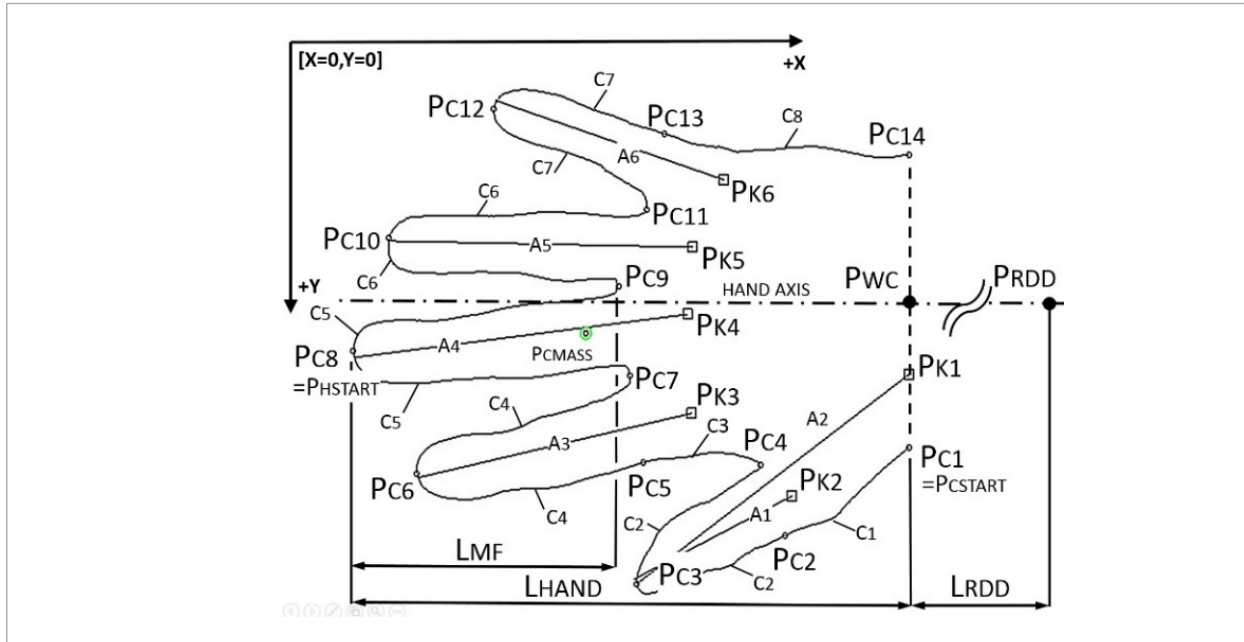


Figure 3

Fully classified hand contour with marked important points and other description. Scheme of the hand in such a manner of how it was created by the proposed algorithm **eaICP** from RGB image. Coordinate basic origin is top left, X axis is horizontal, Y axis is vertical. Points $P_{C1} - P_{C14}$ are key-points on contour of the hand obtained by procession of the RDD. Points $P_{K1} - P_{K6}$ mean positions of important knuckles in which the simulation of rotation is performed in plane XY . Contour c_2 rotates around the knuckle P_{K2} and this knuckle rotates together with contour c_2^* around the knuckle P_{K1} . Axes $A_1, A_2, A_3, A_4, A_5, A_6$ of individual fingers are obtained by calculation with use of linear regression. Axis of thumb A_2 is obtained by connection of the points P_{C3} and P_{K1} . A point P_{RDD} is point from which Radial Distance Diagram is created. A point P_{WC} is point in the middle of distance between points P_{C1} and P_{C14} . Movement and rotation of whole hand contour relates to point P_{CMASS}



The hand position can be slightly variable in plane XY in a certain range of free space within the capturing chamber; and indeed, with regards to the visual field of the used camera.

The background of the scene is black and dull. The RGB image obtained from the camera is first transformed from RGB to HSB model and then to B&W image $I_{B\&W}$ – see Fig. 1. The basic scheme is identical to [55, 56], but the number of „templates“ or images from which were created model M is equal to one. Conversion to B&W representation is conducted in such way that the homogenous black color of the background is considered as an image and from this image is filtered out the foreground. The foreground is the area which is occupied by the hand. The filtered part then makes a black and white image of inserted hand. With use of

mathematical morphology methods, filtration of input image is then performed with use of set of filtration bitmap filtration masks F . These masks remove all unwilling artifacts from the whole area of the image. After that hand contour C is looked up, which is defined as a set of black pixels P_j^C in the image $I_{B\&W}$ and is defined as:

$$C, C \subset I_{B\&W}, \forall P_j^C, P_j^C \in C \wedge P_j^C = 1$$

$$C = (P_j^C), j \in \mathbb{N}^+, P_j^C \in I_{B\&W}. \tag{1}$$

With use of the c , Radial Distance Diagram (RDD) is created:

$$R_{DD} = (P_j^{RDD}), P_j^{RDD} = d(P_{RDD}, P_j^C), j \in \mathbb{N}^+. \tag{2}$$

The contour C is, with use of RDD, segmented out in such a way that the standalone segments of individual finger contours and parts of the palm can be computed – see Fig. 2. On the RDD curve are found significant points which define finger tips and also roots of fingers (valleys) and the algorithm creates a segmented hand contour C_{RDD} . With use of C_{RDD} , a C_{LR} contour is created which is used in the Linear Regression (LR) algorithm, and axes of individual fingers are computed (for thumb 2 knuckles are computed). The result of all these operations is 8-point clouds representing contours of individual parts of the hand contour – 5 fingers and 3 parts of the palm contour up to the wrist. These 8-point clouds make input information for the evolutionary optimizer in which the reference contour is compared with a contour of a person which is identified. Thanks to contours C_{RDD} and C_{LR} , it is possible to create contour M , which represents a comparative sample and contour S , which represents a compared sample – see (3).

$$\begin{aligned} C_{RDD} &= (c_i^{RDD}), c_i^{RDD}, i \in \langle 1, 8 \rangle, c_i^{RDD} = (P_j^{C_{RDD}}), j \in \mathbb{N}^+ \\ C_{LR} &= (c_i^{LR}), i \in \langle 1, 8 \rangle, c_i^{LR} = (P_j^{C_{LR}}), j \in \mathbb{N}^+ \\ M &= (c_i^M), i \in \langle 1, 8 \rangle, c_i^M = (P_j^M), j \in \mathbb{N}^+ \\ S &= (c_i^S), i \in \langle 1, 8 \rangle, c_i^S = (P_j^S), j \in \mathbb{N}^+ . \end{aligned} \quad (3)$$

Reference contours are marked as models M and are stored in a database in the shape of 8- point clouds + several subsidiary items of information taking into account (18). Inside the classifier, model M is compared with a contour marked as sample S . This sample is obtained by identical steps like model M every time when a person has to be identified. Contour S is moreover trimmed for comparative purposes so that unwilling parts do not affect the process of classification. During the classification process, position and heading of a sample S is changed against M and heading of individual fingers of sample S is changed. This change is done independently for every finger with regard to natural physiological limits. The result of classification is a coefficient similarity between M and S with regard to used metrics. For classification purposes contours M and S are trimmed in a suitable manner. Short sections in the finger valley are omitted in range of 7 percent around the point of root of every finger. Complete non-trimmed contour M will be

marked as M_{co} and contours for which the trimming rule was applied will be marked as M_{ea}, S_{ea} . This marking is used in the section of experimental results. The purpose of such a trimming operation is to reach significantly better results. Individual segments c_i^M, c_i^S according to (3) differ from segments c_i^{LR} , which are used in linear regression. For LR operation individual segments are trimmed by 5 percent. LR enables finding axes of individual fingers.

The next part is description of evolutionary process and function. Let's mark the evolutionary process with use of evolutionary optimizer \mathfrak{S}_{EA} and thus we can write:

$$\varepsilon = \arg \underset{H \in \mathbb{R}, S}{opt} \mathfrak{S}_{EA} (M, S, H) . \quad (4)$$

The aim of the evolutionary process (task of optimizer) is to find such value ε , for which holds that $\varepsilon \cong 0$. Of course, this holds only in the case that only two identical contours are compared or. The value ε is equal to value *fitness* according to (5) for only one optimal alignment of contours M and S . Metrics of the *fitness* function was elected based on practical experiments. The *fitness* function utilizes Euclidean distance of contours M and S and also information of topology of some important points $P_{C7}^M, P_{C9}^M, P_{C11}^M$ which are on the hand contour – see Fig. 3. The function *fitness* is then given according to (5) as follows:

$$fitness = R_H + \sum_{j=1}^{j=n} R_j , \quad (5)$$

where R_H represents value of objective function (9), which is given by hand topology and heuristic rules (10), (11), (12) a (13), (14), (15) and additional equations (16), (17). R_j means vale of objective function, which is given by geometry of contour S resp. by points P_j^S and is calculated according to rules of the algorithm ICP and with use of classification rule (7) and equation (8) – alignment of two 2D point clouds. For (8) holds that $P_{\min}^M \in M \wedge P_{x,y}^{I_{B\&W}} \in I_{B\&W}$. n in (5) represents number of points of contour S and also holds that $fitness \in \mathbb{R}^{+,0}$, $j \in \mathbb{N}^+$.

$$R_j \begin{cases} d(P_j^S, P_{\Omega}^M)^4 & \text{if } L_1 = true \\ d(P_j^S, P_{\min}^M) & \text{if } L_1 = false \end{cases} , R_j \in \mathbb{R}^{+,0} \quad (6)$$

$$L_1 = \begin{cases} true, & \text{if } x_3 \notin \langle -0.40^{RAD}; +0.40^{RAD} \rangle \\ true, & \text{if } x_{4-8} \notin \langle -0.30^{RAD}; +0.30^{RAD} \rangle \\ true, & \text{if } x_{0,1} \notin \Omega \\ true, & \text{if } x_2 \notin \langle -0.40^{RAD}; +0.40^{RAD} \rangle \\ false, & \text{oth.} \end{cases} \quad (7)$$

$$P_{\min}^M : d(P_{x,y}^{I_{B&W}}, P_{\min}^M) = \min d(P_{x,y}^{I_{B&W}}, P_i^M), \forall x, y \in I_{B&W} \quad (8)$$

$$R_H = r_{h1} + r_{h2} + r_{h3}, R_H \in \mathbb{R}^{+0} \quad (9)$$

$$r_{h1} = \begin{cases} M_{ul1} * d(P_{C7}^M, \overline{P_{C7}^S}) & \text{if } L_2 = true \\ 0 & \text{if } L_2 = false \end{cases} \quad (10)$$

$$r_{h2} = \begin{cases} M_{ul1} * d(P_{C9}^M, \overline{P_{C9}^S}) & \text{if } L_3 = true \\ 0 & \text{if } L_3 = false \end{cases} \quad (11)$$

$$r_{h3} = \begin{cases} M_{ul1} * d(P_{C11}^M, \overline{P_{C11}^S}) & \text{if } L_4 = true \\ 0 & \text{if } L_4 = false \end{cases} \quad (12)$$

$$L_2 = \begin{cases} true & \text{if } d(P_{C7}^M, \overline{P_{C7}^S}) > M_{ul2} * (0.01 * d_{7,9,11}) \\ false & \text{oth.} \end{cases} \quad (13)$$

$$L_3 = \begin{cases} true & \text{if } d(P_{C9}^M, \overline{P_{C9}^S}) > M_{ul2} * (0.01 * d_{7,9,11}) \\ false & \text{oth.} \end{cases} \quad (14)$$

$$L_4 = \begin{cases} true & \text{if } d(P_{C11}^M, \overline{P_{C11}^S}) > M_{ul2} * (0.01 * d_{7,9,11}) \\ false & \text{oth.} \end{cases} \quad (15)$$

$$d_{7,9,11} = d(P_{C7}^M, P_{C9}^M) + d(P_{C9}^M, P_{C11}^M) \quad (16)$$

$$P_{C...}^S = R(P_{C...}^S - P_{CMASS}^S) + t, t \equiv P_{CMASS}^M + [x_0, x_1] \quad (17)$$

$$D_{ist}(x, y) = \begin{bmatrix} d(P_{x,y}^{I_{B&W}}, P_{\min}^M)_{(0,0)} & \dots & d(P_{x,y}^{I_{B&W}}, P_{\min}^M)_{(x,0)} \\ \dots & \dots & \dots \\ d(P_{x,y}^{I_{B&W}}, P_{\min}^M)_{(0,y)} & \dots & d(P_{x,y}^{I_{B&W}}, P_{\min}^M)_{(x,y)} \end{bmatrix}. \quad (18)$$

P_j^S is j-th point of contour S , P_{\min}^M means a point of contour M , which in sense of used metrics is closest to point P_j^S of contour S with regard to values of genes of chromosome X_i . $\overline{P_{C...}^S}$ means positions of points

$P_{C7}^S, P_{C9}^S, P_{C11}^S$ with regard to actual values of genes $x_{0,1,2}$ of chromosome X_i . R in (17) is a rotational matrix given by value of gene x_2 of chromosome X_i , t is translational vector given by values of gene $x_{0,1}$ with regard to P_{CMASS}^M and P_{CMASS}^S . Points $P_{C7,9,11}^M$ and $P_{C7,9,11}^S$ are significant points on contours M and S – see Fig. 3. Values $M_{ul1} = 50$ and $M_{ul2} = 20$ are selected constants. Heuristic rule R_H (9) is composed of three parts r_{h1}, r_{h2}, r_{h3} and defines when the penalization of the *fitness* function is activated as a consequence of disagreement of topological features of compared contours. Activation of the rule is given with options marked as L_2, L_3, L_4 . In the case that during the evolution, a point P_j^S of contour S is placed out of space of possible solutions D_{om} , a penalization is elected with use of rule L_1 . L_1 is given as $d(P_j^S, P_{\Omega})^4$, for every such point P_j^S of contour S . $d(\dots)$ means Euclidean metrics. Calculation according to (5) is processed for all points in individual selected segments c_i^S of the contour S . Values of matrix D_{ist} are calculated for every contour M and for every point $P_{x,y}^{I_{B&W}}$ of the image $I_{B&W}$ and define the distance of a point $P_{x,y}^{I_{B&W}}$ to the closest point P_i^M of contour M in sense of Euclidean metrics – see also (8). Such a point is marked as P_{\min}^M . Structure of the ICP algorithm is not modified/touched by this step.

Complexity of the original ICP algorithm – see [43] is, for worst case, equal to $O(NM)$ or $O(N^2)$, where N is number of points in contour S and M is number of points in contour M . To cut down huge computational demands even more, the matrix $D_{ist}(x, y)$ was introduced – see (18), (8). Into the matrix $D_{ist}(x, y)$ are stored the values of $d(P_{x,y}^{I_{B&W}}, P_{\min}^M)$ in advance for every point of the image $I_{B&W}$ and for the given corresponding contour M . M in turn, is sketched into the image $I_{B&W}$. Let's define values κ_M, κ_S , which mark what point of a contour will be used for calculation. Corresponding values η_M, η_S , define how many points of a contour is used for calculation with regard to values κ_M, κ_S . Complexity of the proposed **eaICP** algorithm, which, with use of the evolutionary optimizer, aligns two contours M and S is given as follows:

$$O(G_{en} \times N_{pop} \times \eta_s) \approx O(N), \quad (19)$$

where G_{en} means number of generations of evolution algorithm necessary to reach optimal solution, N_{pop} means number of an individual in population P_{op}

of evolutionary algorithm and η_s is assumed as constant for whole time of evolution. Values G_{en} and N_{pop} are in an ideal case also constant for whole computation time.

Practical realization of the algorithm **eaICP** is constructed in such way that optimizer EPSDE calculates objective function according to (5) and with use of matrix D_{ist} . Arrangement of every chromosome X_i is as follows: x_0 - movement of whole contour in axis X, x_1 - movement of whole contour in axis Y, x_2 - heading of whole contour towards axis X in radians, x_{3-8} - rotation of individual fingers in knuckles P_{K1-6} in radians. Angle of heading is limited by (7). Before calculation of objective function, it is necessary to engage the ICP algorithm to align contours of one step. One generation of EA means one iteration step of ICP. EPSDE modifies heading of individual fingers and heading of whole hand and position of whole hand in plane XY. Every iteration of algorithm ICP changes the position of point clouds of contours and S (resp. M_{co}, M_{ea}, S_{ea} according to elected arrangement) – see (17). Both algorithms EPSDE and ICP and objective function (5) are mutually interconnected.

4. Experimental Results

The paragraph of experimental results is divided into several sections: A: time demands of used evolutionary optimizers, B: election of suitable evolutionary optimizer, C: Election of working parameters and accuracy of calculation, D: way of classification, elected assemblages of estimators, E: Results of classification with use of estimator **eaICP** and comparison with other works.

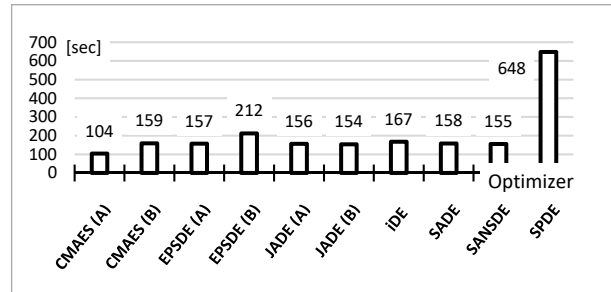
4.1. Time Demands of Used Evolutionary Optimizers

Samples from database THID, image resolution 640x480. Used images THID: **P001-03-M vs. P001-03-S**, $\kappa_M, \kappa_S = 4$. Results – see Fig. 4: **CMA-ES (A)**: $\lambda = 20$, $\mu = 10$, $\sigma = 0.9$, $G_{en}^{CMA-ES} = 200$; **CMA-ES (B)**: $\lambda = 20$, $\mu = 10$, $\sigma = 0.9$, $G_{en}^{CMA-ES} = 300$; **EPSDE (A)**: $N_{pop}^{EPSDE} = 15$, $G_{en}^{EPSDE} = 200$, $L_p^{EPSDE} = 10$; **EPSDE (B)**: $N_{pop}^{EPSDE} = 20$, $G_{en}^{EPSDE} = 200$, $L_p^{EPSDE} = 10$; **JADE (A)**: $N_{pop}^{JADE} = 15$, $G_{en}^{JADE} = 200$, $c^{JADE} = 0.1$, $p^{JADE} = 0.05$, with archive; **JADE (B)**: without archive; **jDE**: $N_{pop}^{jDE} = 15$,

$G_{en}^{jDE} = 200$, $\tau_1^{jDE} = 0.9$, $\tau_2^{jDE} = 0.2$, $f_u^{jDE} = 0.7$, $f_l^{jDE} = 0.3$; **SADE**: $N_{pop}^{SADE} = 15$, $G_{en}^{SADE} = 200$, $L_p^{SADE} = 10$; **SANSDE**: $N_{pop}^{SANSDE} = 15$, $G_{en}^{SANSDE} = 200$, $L_p^{SANSDE} = 10$, $f_p^{SANSDE} = 0.5$; **SPDE**: $N_{pop}^{SPDE} = 40$, $G_{en}^{SPDE} = 300$, $F^{SPDE} = \langle 0.00001, 2 \rangle$, $P_{cx}^{SPDE} = \langle 0.00001, 1 \rangle$, $\kappa_M, \kappa_S = 4$. Calculations of time demand were performed with use of 6 core processor AMD-fx-6100-3.3GHz. Used algorithm development is in MSVS2008SP1-C++/CLI-.NET3.5, 32bit task.

Figure 4

Time demands of tested optimizers at comparison of two samples



4.2. Election of Suitable Evolutionary Optimizer

Eleven carefully selected optimizers were tested if they are suitable for solving a given optimization task: CMA-ES, EPSDE, JADE, jDE, SADE, SANSDE, SPDE and marginally also PSO, RPSO, SGA and PBO. For test purposes, the **eaICP** optimizer was elected which uses *fitness* calculation without the matrix D_{ist} . During tests hand images/contours were used and marked as THID: M : P001-03-M and S P001-03-S, but for M positions of all points P_k for all fingers were changed. The contour stayed identical. P001 marks number of person in database, -03- marks number of image from every person in range 1 to 10 images. Positions of points P_k were changed a bit in such way that final *fitness* was not equal to zero and the optimizer has the more complicated task to solve. E.g. for little finger M: $P_{K6}, x = 346.97181$, $P_{K6}, y = 151.68178$ and position of corresponding knuckle S: $P_{K6}, x = 346.87492$, $P_{K6}, y = 151.33841$. Thanks to such modification many narrowly bordered optimums arise around the ideal pose. At tests, values $\kappa_M, \kappa_S = 4$ -th sample of contours M and S was used. In an ideal case the ideal *fitness* value has to be equal to zero. The error in order of individual pixels is not substantial. Hence in order to compare individual optimizers, identical number of indi-

viduals and generations were elected: $G_{en} = 200, N_{pop} = 15$. For CMA-ES then $\lambda = 20, \mu = 10, \sigma = 0.9$. Value $G_{en} = 200$ is elected regarding to time limitations and size of used databases THID, GPDS. In images, convergence of population for 100x repeating trial is recorded, and also best reached value *fitness* in individual iterations. Because used EAs have different working parameters, only the combination which led to best results was elected. Final results are recorded in Fig. 5-11. Working parameters of individual EAs are recorded too. It is visible, that the best results were provided by the EPSDE optimizer – see Fig. 6. On second place tightly follows jDE optimizer – see Fig. 8. EPSDE and jDE show both only small differences, but EPSDE is better although only about 5-7 percent.

Figure 5

Optimizer **CMA-ES**:

$$\lambda = 20, \mu = 10, \sigma = 0.9, G_{en}^{CMA-ES} = 200, \kappa_M, \kappa_S = 4$$

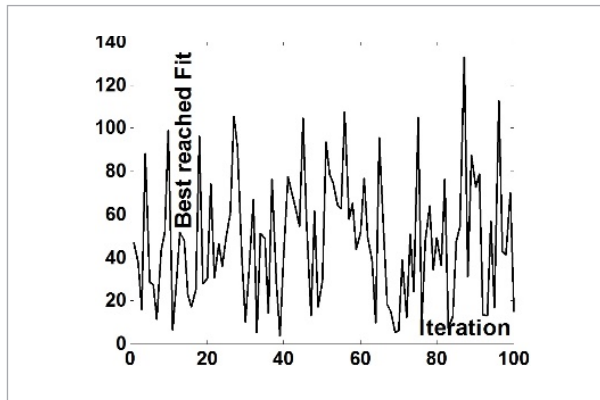


Figure 6

Optimizer **EPSDE**.

$$N_{pop}^{EPSDE} = 15, G_{en}^{EPSDE} = 200, L_p^{EPSDE} = 10, \kappa_M, \kappa_S = 4$$

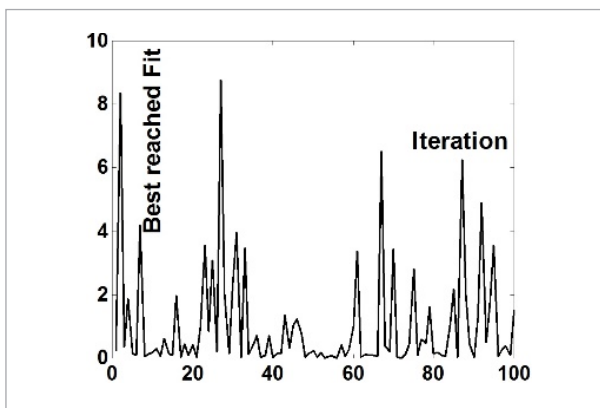


Figure 7

Optimizer **JADE**.

$N_{pop}^{JADE} = 15, G_{en}^{JADE} = 200, c^{JADE} = 0.1, p^{JADE} = 0.05$, with archive. “with archive” and “without archive” – almost identical results $\kappa_M, \kappa_S = 4$

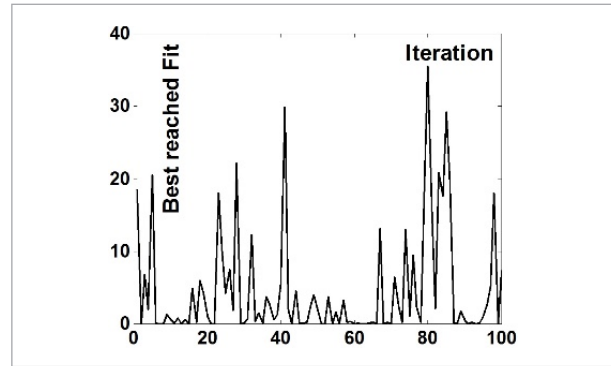


Figure 8

Optimizer **jDE**.

$$N_{pop}^{jDE} = 15, G_{en}^{jDE} = 200, \tau_1^{jDE} = 0.9, \tau_2^{jDE} = 0.2, f_u^{jDE} = 0.7, f_l^{jDE} = 0.3, \kappa_M, \kappa_S = 4$$

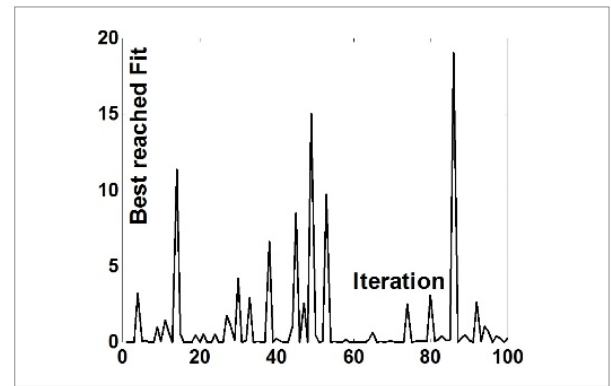


Figure 9

Optimizer **SADE**.

$$N_{pop}^{SADE} = 15, G_{en}^{SADE} = 200, L_p^{SADE} = 10, \kappa_M, \kappa_S = 4$$

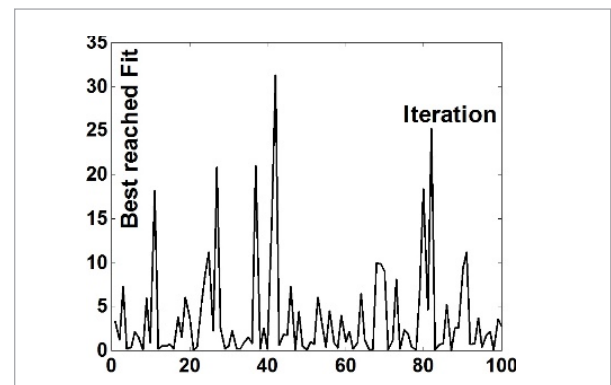


Figure 10

Optimizer **SANSDE**.

$$N_{pop}^{SANSDE} = 15, G_{en}^{SANSDE} = 200, L_p^{SANSDE} = 10, f_p^{SANSDE} = 0.5, \kappa_M, \kappa_S = 4$$

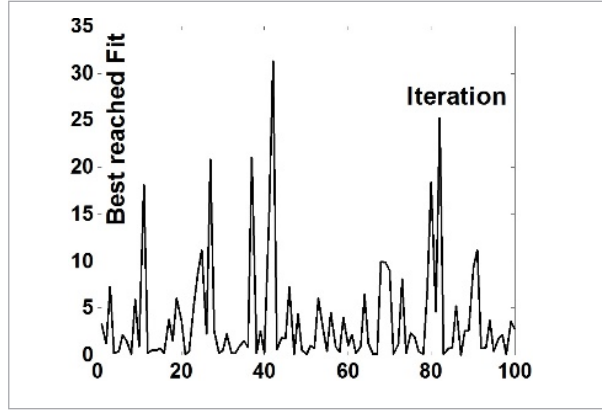
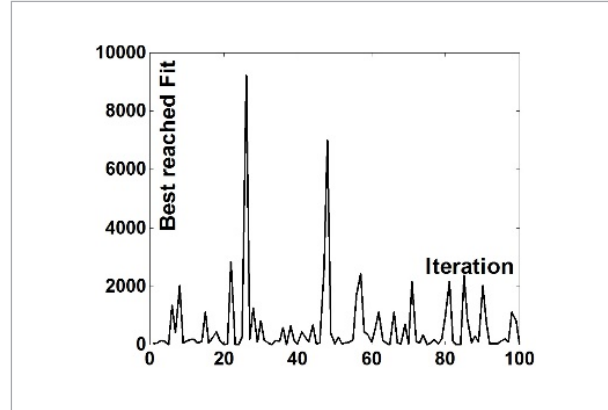


Figure 11

Optimizer **SPDE**.

$$N_{pop}^{SPDE} = 40, G_{en}^{SPDE} = 300, F^{SPDE} = \langle 0.00001, 2 \rangle, P_{cx}^{SPDE} = \langle 0.00001, 1 \rangle, \kappa_M, \kappa_S = 4$$



Other places took algorithms SADE – see Fig. 9, JADE – see Fig. 7 and there is no difference between JADE with archive and without archive, SANSDE – see Fig. 10 and CMA-ES – see Fig. 5. SPDE recorded very bad results – see Fig. 11, which shows very frequent sticking in a local optimum. Algorithms JADE, jDE, SADE, EPSDE and SANSDE are very similar to each other for converge to optimal solution. Big differenc-

es occurred in the last 50 generations where the best solution of a given task is capable of finding only jDE and EPSDE algorithms. A big disappointment was CMA-ES. Convergence speed is large – see Fig. 5. After 100-120 generations, it reaches relatively good value of *fitness*, but next decrease of *fitness* to zero is a huge problem. CMA-ES is not suitable to solve this problem.

Figure 12

The chart of progress at estimation of accuracy of proposed method for various values κ_M, κ_S . In first step is ascertained value *fitness* for $\kappa_M, \kappa_S = 1$, then value κ_M, κ_S is changed in given range and vector X_i is inserted back to algorithm **eaICP** with coefficients $\kappa_M, \kappa_S = 1$ and final *fitness* is calculated. Used samples THID: **P001-03-M** and **P057-08-S** (smaller hand)

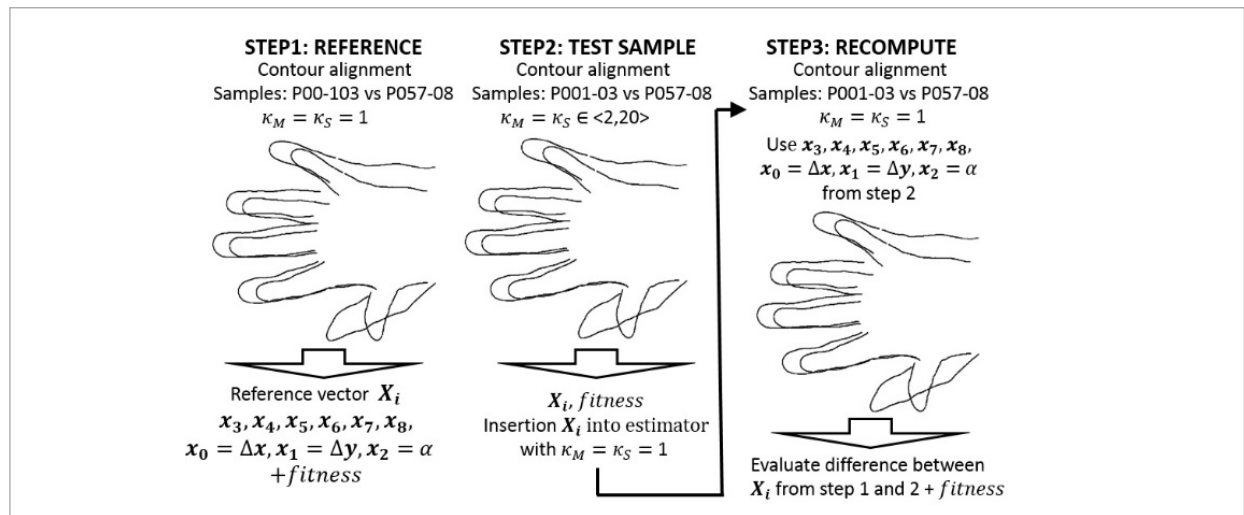


Figure 13

Top-attained values *fitness* for gradually increasing values κ_M, κ_S . Samples THID: **P001-03-M** and **P057-08-S**. vector X_i was after calculation inserted back to estimator with parameters $\kappa_M, \kappa_S = 1$ and then was estimated the final *fitness*. $\kappa_M, \kappa_S = 1$ is reference sample. **Bottom**-difference between *fitness* = 26526.5 for $\kappa_M, \kappa_S = 1$ and *fitness*, which was obtained for actually tested value κ_M, κ_S . (dotted line is the trend)

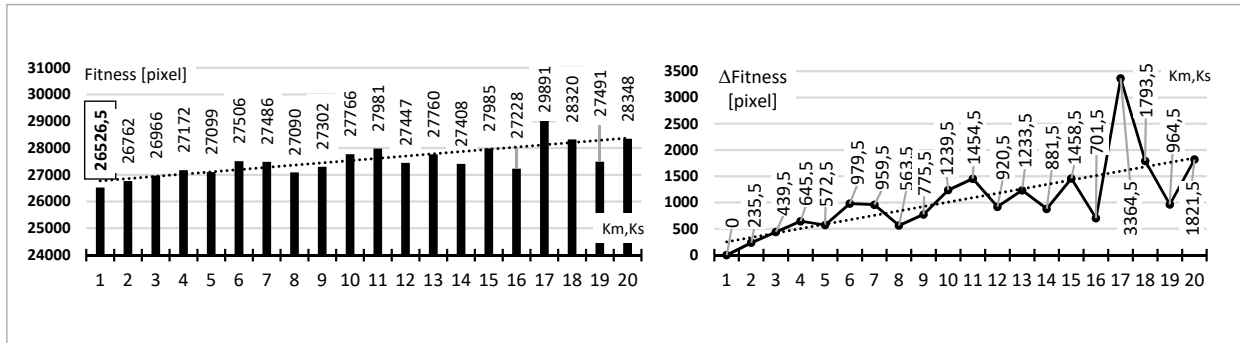


Table 1

Elected assemblages A1-A11 of evolutionary estimators. $c_{4-8}^{M_{ev}}, c_{4-8}^{S_{ev}}$ – marking of contours used at classification. Marking R_H, R_I is according to (5). In some experiments are omitted heuristic rules R_H and *fitness* is calculated with use of rule R_I . P_{K1-6} – means numbers of knuckles of individual fingers – see Fig. 2, which participates at calculation according to Fig. 1. Ex – means the number of the estimator (algorithm) according to [60]

Asm.	Database, image resolution, used contours, num. of fingers, classifier rules, used knuckles, num. of dimensions, estimator name	Asm.	Database, image resolution, used contours, num. of fingers, classifier rules, used knuckles, num. of dimensions, estimator name
A1	THID, 1280x960, $c_{4-8}^{M_{ev}}, c_{4-8}^{S_{ev}}$, 4 fingers, $R_H + R_I, R_{K3-6}$, $D_{im} = 7, E9$	A7	THID, 640x480, $c_{1-8}^{M_{ev}}, c_{1-8}^{S_{ev}}$, 5 fingers, $R_H + R_I, P_{K1-6}$, $D_{im} = 9, E8$
A2	THID, 1280x960, $c_{4-8}^{M_{ev}}, c_{4-8}^{S_{ev}}$, 4 fingers, $R_H + R_I, P_{K3-6}$, $D_{im} = 7, E9$	A8	GPDS, 1403x1021, $c_{4-8}^{M_{ev}}, c_{4-8}^{S_{ev}}$, 4 fingers, $R_H + R_I, P_{K3-6}$, $D_{im} = 7, E9$
A3	THID, 1280x960, $c_{4-7}^{M_{ev}}, c_{4-7}^{S_{ev}}$, 4 fingers, R_I, P_{K3-6} , $D_{im} = 7, E5$	A9	GPDS, 640x480, $c_{1-8}^{M_{ev}}, c_{1-8}^{S_{ev}}$, 5 fingers, R_I, P_{K1-6} , $D_{im} = 9, E3$
A4	THID, 640x480, $c_{4-8}^{M_{ev}}, c_{4-8}^{S_{ev}}$, 4 fingers, $R_H + R_I, P_{K3-6}$, $D_{im} = 7, E9$	A10	GPDS, 640x480, $c_{1-8}^{M_{ev}}, c_{1-8}^{S_{ev}}$, 5 fingers, $P_{K1,3-6}, P_{K2}$ fixed, $D_{im} = 8, E11$
A5	THID, 640x480, $c_{4-7}^{M_{ev}}, c_{4-7}^{S_{ev}}$, 4 fingers, $R_H + R_I, P_{K3-6}$, $D_{im} = 7, E10$	A11	GPDS, 640x480, $c_{4-8}^{M_{ev}}, c_{4-8}^{S_{ev}}$, 4 fingers, $R_H + R_I, P_{K3-6}$, $D_{im} = 7, E9$
A6	THID, 640x480, $c_{1-8}^{M_{ev}}, c_{1-8}^{S_{ev}}$, 5 fingers, $R_I, P_{K1,3-6}, P_{K2}$ fixed, $D_{im} = 8, E11$		

Description of individual marking Ex with regard to assemblages A1 to A11 used in algorithm [64]:

Mark of eaICP estimator E3, 9 dim task:

$x_0, x_1, x_2, x_3, x_4, x_5, x_6, x_7, x_8$; all contours $c_1^{\dots}, c_2^{\dots}, c_3^{\dots}, c_4^{\dots}, c_5^{\dots}, c_6^{\dots}, c_7^{\dots}, c_8^{\dots}$ are used in calculation and corresponding knuckles P_{K1-6} i.e. all 5 fingers, only the rule R_i is used in calculation *fitness* according to (5).

Mark of eaICP estimator E5, 7 dim task:

$x_0, x_1, x_2, x_3, x_4, x_5, x_6, x_7, x_8$; the knuckles P_{K1}, P_{K2} are omitted from calculation and also corresponding contours $c_1^{\dots}, c_2^{\dots}, c_3^{\dots}$; contours which participate in calculation $c_4^{\dots}, c_5^{\dots}, c_6^{\dots}, c_7^{\dots}, c_8^{\dots}$ and knuckles P_{K3-6} , only rule R_i is used in calculation of *fitness* value according to (5).

Mark of eaICP estimator E8, 9 dim task:

$x_0, x_1, x_2, x_3, x_4, x_5, x_6, x_7, x_8$; the contours which participate in calculation $c_1^{\dots}, c_2^{\dots}, c_3^{\dots}, c_4^{\dots}, c_5^{\dots}, c_6^{\dots}, c_7^{\dots}, c_8^{\dots}$ and corresponding knuckles P_{K1-6} i.e. all 5 fingers, the classification rules $R_H + R_i$ are used to calculate the value *fitness* according to (5).

Mark of eaICP estimator E9, 7 dim task:

$x_0, x_1, x_2, x_3, x_4, x_5, x_6, x_7, x_8$; the knuckles P_{K1}, P_{K2} are omitted from calculation and also corresponding contours $c_1^{\dots}, c_2^{\dots}, c_3^{\dots}$; the contours which participate in calculation $c_4^{\dots}, c_5^{\dots}, c_6^{\dots}, c_7^{\dots}, c_8^{\dots}$ and knuckles P_{K3-6} , it uses the rules $R_H + R_i$ to calculate *fitness* value according to (5).

Mark of eaICP estimator E10, 7 dim task:

$x_0, x_1, x_2, x_3, x_4, x_5, x_6, x_7, x_8$; the knuckles P_{K1}, P_{K2} are omitted from calculation and also corresponding contours $c_1^{\dots}, c_2^{\dots}, c_3^{\dots}$ the contour c_8^{\dots} is also omitted; the contours which participate at calculation $c_4^{\dots}, c_5^{\dots}, c_6^{\dots}, c_7^{\dots}$ and knuckles P_{K3-6} , it uses both the classification rules $R_H + R_i$ in calculation of *fitness* according to (5).

Mark of eaICP estimator E11, 8 dim task:

$x_0, x_1, x_2, x_3, x_4, x_5, x_6, x_7, x_8$; the knuckle P_{K2} is fixed; the contours which participate in calculation $c_1^{\dots}, c_2^{\dots}, c_3^{\dots}, c_4^{\dots}, c_5^{\dots}, c_6^{\dots}, c_7^{\dots}, c_8^{\dots}$ and corresponding knuckles $P_{K1,3-6}$ i.e. all 5 fingers, only the rule R_i is used in calculation of value *fitness* according to (5).

Marginally were also tested optimizers PSO, RPSO. Unfortunately, both are not suitable to solve the given task. The SGA optimizer was also tested with a chromosome which is expressed as the chain of bits of length of chromosome/gene 136/17 bits, $N_{pop}^{SGA} = 20$, $G_{en}^{SGA} = 200$, accuracy 1×10^{-5} and with various types of evolutionary operators. SGA enables very fast starting convergence and behaves like CMA-ES, but it has big problem to find an accurate solution and gets stuck in local optima very often or convergence fails totally.

Just the random malfunctions of convergence to optimal solution makes the SGA scarcely usable. A metaheuristic optimizer PBO was also tested which is a

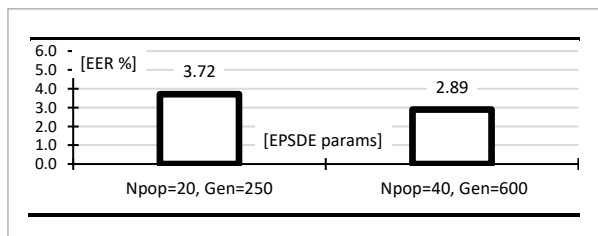
newbie in the optimization sphere but its efficiency at solving of 7, 8 and primarily 9-dimensional optimization tasks is very bad. PBO shows 50 percent worse results and primarily thanks to its internal arrangement, is 3x slower in comparison to EPSDE. Such classifier is unusable. As the most suitable optimizer, the EPSDE algorithm was selected.

4.3. Election of Working Parameters, Accuracy of Calculation

Selected optimizer EPSDE has only one working parameter L_p^{EPSDE} . For correct operation it is necessary to also find the correct number of individuals in the population, the number of generations as termination condition, and values η_M, η_S resp. κ_M, κ_S . Based on the performed experiment it was ascertained that parameter L_p^{EPSDE} has only very small effect on the result of optimization, hence for all calculations was set to value 10. Convergence curves of the EPSDE are smooth and without any unwilling peaks. Selection of values κ_M, κ_S were processed with regard to technical possibilities and accuracy of final result. For tests two images from database THID were selected, and marked as P001-03-M and P057-08-S – see Fig. 12. One bigger and one smaller contour were selected, so it was evident that there is no unambiguous correspondence at alignment. Hence in order for it to be possible to

Figure 14

Effect of values $N_{pop}^{EPSDE}, G_{pop}^{EPSDE}$ on final value EER% for 108160 evolutions resp. contour alignments. Database THID, 640x480, contours c_{4-7}^{M}, c_{4-7}^{S} , 4 fingers, $R_i, D_{im} = 7$



ascertain minimal values κ_M, κ_S usable for next experiments, both contours were aligned for $\kappa_M, \kappa_S = 1$. The used **eaICP** algorithm, with parameters $N_{pop}^{EPSDE} = 20$, $G_{en}^{EPSDE} = 500$, and $L_p^{EPSDE} = 10$, then calculated values x_j of vector u X_i . Number of repetitions was 10. Average value of *fitness* was also calculated equal to 26526,50 pixels from these 10 repetitions. After that the trial was performed for row of values $\kappa_M, \kappa_S \in \langle 2, 20 \rangle$ with step 1 and setting of EPSDE: $N_{pop}^{EPSDE} = 15$, $G_{en}^{EPSDE} = 200$, $L_p^{EPSDE} = 10$. Every trial was again repeated 10x. Resulting values were recorded and average value calculated from genes x_j of the chromosome X_i from the 10 repetitions for individual $\kappa_M, \kappa_S \in \langle 2, 20 \rangle$ was again inserted back as a correct solution into algorithm **eaICP**, where $\kappa_M, \kappa_S = 1$ and the *fitness* was calculated – see Fig. 13. According to presupposition, the *fitness* value was gradually slowly increasing at increasing values κ_M, κ_S . The proposed estimator is considerably stable. Based on extensive experiments see Fig. 5-11, the EPSDE optimizer was selected as the best optimizer from the group of tested optimizers – the optimizer shows the smallest number of malfunctions at convergence and contains only a minimal number of working parameters. The only useful values were N_{pop}^{EPSDE} and G_{en}^{EPSDE} . These values have to be set manually and, according to expectations, depend on image resolution and number of pixels of hand contour. For image resolution 640x480 pixels are good enough values $N_{pop}^{EPSDE} = 15 - 20$, $G_{en}^{EPSDE} = 200$, $L_p^{EPSDE} = 10$. Unfortunately, at experiments it was proved that at large number of repetitions in order of ten thousand, imperfect convergence for EPSDE can occur. Complete processing of the database THID requires 108160 contour alignments. Total malfunction similar to SGA is, indeed, not observed but the final value for every thousand evolutions does not reach an ideal value at contour alignment. This effect is visible for coefficient *EER*. This effect is recorded in Fig. 14 and has universal character for all image resolutions. Difference between ideal values of *EER* at large number of evolutions is however small cca 0.1%, but visible. To reach better values it is possible to increase the number of individuals in the population and also the number generations to e.g. $N_{pop}^{EPSDE} = 40$, $G_{en}^{EPSDE} = 600$.

For experimental purposes following arrangements of contours, image resolution and classification criteria (5) were elected see Tab. 1. Individual assemblages

of estimators are marked as A1-11. The type of used database is also noted. The type of contours M and S at experiments, and number of contours are used according to (3). The number of fingers, and type of used classification criteria is according to (5). All knuckles are included into the calculation – see Fig. 3. The number of dimensions of the task and also number of estimators are according to algorithm in [60]. In Tables 8-19 are recorded all important results and statistical values ΣI_{UL} , *FAR*%, ΣG_{OL} , *FRR*% and *EER*%. Point *EER* is recorded in percent and also in pixels. Individual assemblages A1-A11 – see Tab. 1, use different types of contours which are marked as M_{co}, M_{ea}, S_{ea} . Based on practical experiments, it was ascertained that during the comparison of trimmed and non-trimmed contours M_{co}, S_{ea} , it is possible to attain significantly better results even with use of only one template M_{co} or M_{ea} from every person (genuine). For classification purposes *FAR* (False Acceptance Rate) values, *FRR* (False Rejection Rate) and point *EER* (Equal Error Rate point or Equilibrium) are used – see e.g. (Sanches-Reillo et al. 2000) according to (20, 21, 22):

$$FAR = \frac{\Sigma I_{UL}}{\Sigma I_{TOT}}, FRR = \frac{\Sigma G_{OL}}{\Sigma G_{TOT}} \quad (20)$$

Database THID:

$$\Sigma G_{TOT} = 104 \times 10 = 1040 \quad (21)$$

$$\Sigma I_{TOT} = 108160 - 1040 = 107120$$

Database GPDS:

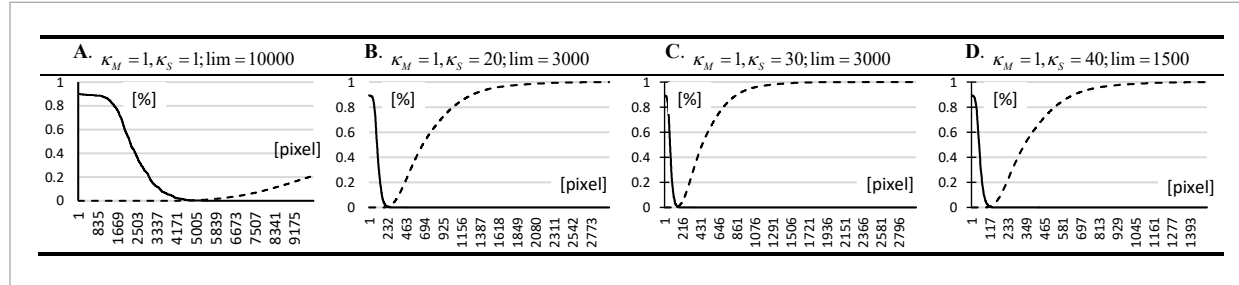
$$\Sigma G_{TOT} = 94 \times 10 = 940 \quad (22)$$

$$\Sigma G_{TOT} = 88360 - 940 = 87420,$$

where ΣG_{OL} – sum of all genuine samples for which exceeded the required limit λ_{EER} , ΣG_{TOT} – total number of genuine samples, ΣI_{UL} – number of impostors, which thanks to malfunction of classifier fall under predefined value λ_{EER} , ΣI_{TOT} – total number of impostors. Value λ_{EER} represents the found point of equilibrium in pixels. Several experiments were performed with various values $\kappa_S \in \langle 1, 5, 10, 15, 20, 25, 30, 35, 40 \rangle$, in order to ascertain how stable and robust are the proposed estimators. Any value κ_S greater than 1 almost always led to worse results. Value κ_M greater than 1 eminently always led to worse results and hence only value $\kappa_M = 1$ was always used.

Figure 15

Selected curves FAR , FRR for selected values κ_s and for results in Tab. 2. Key: - - - FAR — FRR , **eaICP**, Vertical axis is in percent in range $\langle 0,0.1.0 \rangle$. Horizontal axis gives value $fitness$ in pixels or interval $\langle 0, \lambda_{EER} \rangle$ in which the EER value is sought. THID database



4.5. Results of Classification with Use of Estimator eaICP and Comparison with Other Works

In Tab. 8-19 are recorded all results for elected assemblages A1-A12 of estimator **eaICP** – see Tab. 1. All calculations were performed with use of the matrix D_{lst} – see (5). First will be presented results for database THID (104 persons - genuine x 1040 images impostors + genuine, 10 images of every person, totally 108160 comparisons) and corresponding estimator assemblages A1-A7 and various combinations of types of contours and number of fingers. The best results of **eaICP** algorithm at work with database

THID were reached for assemblage A1: $FAR = 0.38\%$, $FRR = 0.38\%$, $EER = 0.38\%$, $IR = 99.61\%$ - see Tab. 2 and Fig. 15, 16. Value A1: $EER = 0.38\%$, is not “totally” ideal. The reason is that e.g. person P055 in images P055-09, P55-10 incorrectly placed his hand to the pad – fingers were unnaturally bent at angle 70 of degrees etc. [8] attained using identical database a best result of $EER = 0.52\%$ with use of LDA algorithm and with use of standalone Euclidean rule, only a value of $EER = 3.5\%$ – see Tab. 13. In Tab. 3 are recorded results for assemblage A2: $FAR = 0.48\%$, $FRR = 0.48\%$, $EER = 0.48\%$. These results are still better than [8] attained using LDA algorithm. A value of $EER = 0.48\%$

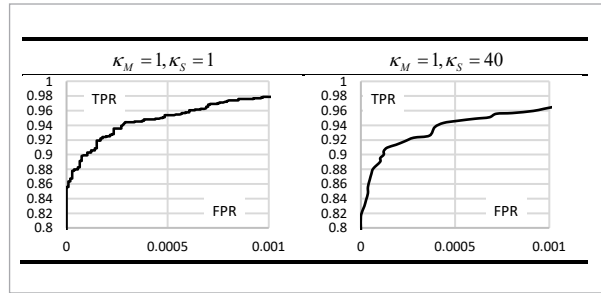
Table 2

Statistics of success rate of estimator A1, values FAR , FRR , EER , viz Tab. 1, A1: THID, 1280x960, $c_{4-8}^{M_{co}}$, $c_{4-8}^{S_{ea}}$, 4 fingers, $R_H + R_I$, R_{K3-6} , $D_m = 7$, E9. Time demands in [sec.ms] are assumed for successful alignment of samples THID: **P001-03-M a P057-08-S** – samples see Fig. 12. Total number of evolutions is: 9 rows x 108160 comparisons M_{co} vs $S_{ea} = 973\,440$ evolutions. For row 1 is the value of Identification rate (IR) equal to 99.61%. $N_{pop}^{EPSDE} = 40$, $G_{en}^{EPSDE} = 420$

n.	κ_M	κ_S	ΣI_{UL}	$FAR\%$	ΣG_{OL}	$FRR\%$	$ERR\% / \text{pixel}$	Tot. time
1	1	1	412	0.38	4	0.38	0.38 / 4873	23.340
2	1	5	615	0.57	6	0.57	0.57 / 965	5.240
3	1	10	614	0.57	6	0.57	0.57 / 476	2.790
4	1	15	512	0.47	5	0.48	0.47 / 309	1.990
5	1	20	427	0.39	4	0.38	0.38 / 226	1.540
6	1	25	613	0.57	6	0.57	0.57 / 189	1.290
7	1	30	563	0.52	5	0.48	0.52 / 155	1.140
8	1	35	599	0.55	6	0.57	0.55 / 133	1.000
9	1	40	680	0.63	7	0.67	0.63 / 118	0.920

Figure 16

Selected Receive Operating Characteristics - ROC curves for estimator A1. ROC curves are for values in Tab. 2 i.e. for estimator. A1: THID, 1280x960, $c_{4-8}^{M_{co}}, c_{4-8}^{S_{ea}}$, 4 fingers, $R_H + R_I$, $P_{\kappa_{3-6}}, D_{im} = 7, E9$. Horizontal axis-False Positive Rate (FPR), Vertical axis-True Positive Rate (TPR)



for assemblage A2 is worse in comparison to A1, because contours M_{ea}, S_{ea} were compared. For assemblage A3, Tab. 4 the **eaICP** estimator recorded final values A3: $FAR = 1.92\%, FRR = 1.92\%, EER = 1.92\%$. Only Euclidean criteria R_I was used during calculations – see (5). The reason of worse result than for A1 is that ICP algorithm without any support of heuristic rules R_H has not such efficiency. The difference in assemblage A1 and A3 is that for A3 part of contour from little finger to wrist was omitted. The fact that this part of the hand contour is important was ascertained based on experiments. This is visible from results in Tab. 2 and Tab. 4. For assemblage A4 was at-

tained values $FAR = 1.15\%, FRR = 1.15\%, EER = 1.15\%$ for A5: $FAR = 1.83\%, FRR = 1.82\%, EER = 1.83\%$, for A6: $FAR = 3.49\%, FRR = 3.46\%, EER = 3.49\%$ and finally for A7: $FAR = 1.82\%, FRR = 1.82\%, EER = 1.82\%$. Assemblage A4 works with 4 fingers and uses both classification criteria. Assemblage A5 is identical to A4, but part of hand contour between little finger and wrist is omitted. Assemblage A6 works with 5 fingers but the thumb has only one knuckle. Hence, all results are markedly worse. In assemblage A7, the thumb has two knuckles. Thanks to that the final result is significantly better in comparison to A6. From results in Tab. 4,5,6 for assemblage A3, A4, A5, it follows that the final value EER has big effect on the type of compared contours M_{co}, M_{ea}, S_{ea} . The best results can be reached just for combination of contours M_{co}, S_{ea} and at use of both classification criteria $R_H + R_I$ according to (5). The estimator which uses contours M_{ea}, S_{ea} is also less robust. This fact is highly visible at comparison of results for $\kappa_S = 1 - 40$. For all estimators where only the R_I rule is used, without R_H , worse results were reached. The rule of guaranteed convergence of the ICP algorithm holds for identical or “almost” identical point clouds. In the case of classification of set of points which makes a hand contour with use of the ICP algorithm, the favored position of alignment of contour M and S is in direction to end of fingers, where there is larger number of points than in the

Table 3

Statistics of success rate of estimator A2, values FAR, FRR, EER , see Tab. 1. A2: THID, 1280x960, $c_{4-8}^{M_{co}}, c_{4-8}^{S_{ea}}$, 4 fingers, $R_H + R_I$, $P_{\kappa_{3-6}}, D_{im} = 7, E9$. Time demands in [sec.ms] are assumed for successful alignment of samples THID: **P001-03-M** a **P057-08-S** – samples see Fig. 12. Total number of evolutions is: 9 rows \times 108160 comparisons M_{ea} vs $S_{ea} = 973\,440$ evolutions. $N_{pop}^{EPSDE} = 40$, $G_{en}^{EPSDE} = 420$

n.	κ_M	κ_S	ΣI_{UL}	$FAR\%$	ΣG_{OL}	$FRR\%$	$ERR\% / \text{pixel}$	Tot. time
1	1	1	515	0.48	5	0.48	0.48 / 4856	23.180
2	1	5	523	0.48	5	0.48	0.48 / 963	5.160
3	1	10	591	0.55	5	0.48	0.56 / 482	2.770
4	1	15	637	0.59	6	0.57	0.59 / 402	1.980
5	1	20	699	0.65	7	0.67	0.64 / 373	1.530
6	1	25	782	0.73	8	0.76	0.75 / 285	1.290
7	1	30	847	0.79	9	0.86	0.79 / 201	1.120
8	1	35	911	0.85	10	0.96	0.85 / 157	1.000
9	1	40	1079	1.00	10	0.96	1.00 / 132	0.900

Table 4

Statistics of success rate of estimator A3, values FAR , FRR , EER , see Tab. 1. A3: THID, 1280x960, $c_{4-7}^{M_{ea}}$, $c_{4-7}^{S_{ea}}$, 4 fingers, R_l , R_{K3-6} , $D_{im} = 7$, E5. Time demands in [sec.ms] are assumed for successful alignment of samples THID: **P001-03-M** a **P057-08-S** – samples see Fig. 12. Total number of evolutions is: 9 rows \times 108160 comparisons M_{ea} vs $S_{ea} = 973\,440$ evolutions. $N_{pop}^{EPSDE} = 40$, $G_{en}^{EPSDE} = 420$

n.	κ_M	κ_S	ΣI_{UL}	$FAR\%$	ΣG_{OL}	$FRR\%$	$ERR\% / \text{pixel}$	Tot. time
1	1	1	2062	1.92	20	1.92	1.92 / 4572	21.652
2	1	5	2078	1.93	22	2.11	1.93 / 914	4.860
3	1	10	2130	1.98	23	2.21	1.97 / 453	2.610
4	1	15	2243	2.09	26	2.50	2.09 / 342	1.830
5	1	20	2560	2.38	27	2.59	2.38 / 246	1.470
6	1	25	2782	2.59	29	2.78	2.59 / 201	1.210
7	1	30	3078	2.87	30	2.88	2.87 / 189	0.940
8	1	35	3200	2.98	30	2.88	2.98 / 157	0.920
9	1	40	3610	3.37	34	3.26	3.37 / 139	0.870

Table 5

Statistics of success rate of estimator A4, values FAR , FRR , EER , see Tab. 1. A4: THID, 640x480, $c_{4-8}^{M_{co}}$, $c_{4-8}^{S_{co}}$, 4 fingers, $R_H + R_p$, R_{K3-6} , $D_{im} = 7$, E9. Time demands in [sec.ms] are assumed for successful alignment of samples THID: **P001-03-M** a **P057-08-S** – samples see Fig. 12. Total number of evolutions is: 9 rows \times 108160 comparisons M_{co} vs $S_{co} = 973\,440$ evolutions. $N_{pop}^{EPSDE} = 20$, $G_{en}^{EPSDE} = 200$

n.	κ_M	κ_S	ΣI_{UL}	$FAR\%$	ΣG_{OL}	$FRR\%$	$ERR\% / \text{pixel}$	Tot. time
1	1	1	1239	1.15	12	1.15	1.15 / 1248	1.996
2	1	5	1288	1.20	17	1.63	1.20 / 249	0.491
3	1	10	1302	1.21	19	1.82	1.22 / 115	0.296
4	1	15	1478	1.37	22	2.11	1.37 / 98	0.218
5	1	20	2077	1.93	25	2.40	1.95 / 92	0.187
6	1	25	2498	2.33	28	2.69	2.34 / 88	0.171
7	1	30	2870	2.67	29	2.78	2.67 / 62	0.150
8	1	35	3132	2.92	30	2.88	2.92 / 40	0.144
9	1	40	3538	3.33	30	2.88	3.30 / 33	0.140

Table 6

Statistics of success rate of estimator A5, values *FAR*, *FRR*, *EER*, see Tab. 1. A5: THID, 640x480, $c_{4-7}^{M_{co}}$, $c_{4-7}^{S_{ca}}$, 4 fingers, $R_H + R_I$, P_{K3-6} , $D_{im} = 7$, E10. Time demands in [sec.ms] are assumed for successful alignment of samples **THID: P001-03-M** a **P057-08-S** – samples see Fig. 12. Total number of evolutions is: 9 rows \times 108160 comparisons M_{co} vs $S_{ca} = 973\,440$ evolutions. $N_{pop}^{EPSDE} = 20$, $G_{en}^{EPSDE} = 200$

n.	κ_M	κ_S	ΣI_{UL}	<i>FAR</i> %	ΣG_{OL}	<i>FRR</i> %	<i>ERR</i> % / pixel	Tot. time
1	1	1	1963	1.83	19	1.82	1.83 / 1153	1.903
2	1	5	1998	1.86	19	1.82	1.85 / 230	0.483
3	1	10	2002	1.86	22	2.11	1.87 / 164	0.280
4	1	15	2140	1.99	27	2.59	1.97 / 130	0.218
5	1	20	2490	2.32	29	2.78	2.32 / 98	0.171
6	1	25	2673	2.49	30	2.88	2.49 / 74	0.156
7	1	30	2980	2.78	31	2.98	2.78 / 41	0.150
8	1	35	3054	2.85	33	3.17	2.85 / 32	0.144
9	1	40	3139	2.93	34	3.26	2.93 / 27	0.140

Table 7

Statistics of success rate of estimator A6, values *FAR*, *FRR*, *EER*, viz Tab. 1. A6: THID, 640x480, $c_{1-8}^{M_{co}}$, $c_{1-8}^{S_{ca}}$, 5 fingers, R_I , R_{K1-6} , R_{K2} fixed, $D_{im} = 8$, E11. Time demands in [sec.ms] are assumed for successful alignment of samples **THID: P001-03-M** a **P057-08-S** – samples see Fig. 12. Total number of evolutions is: 9 rows \times 108160 comparisons M_{co} vs $S_{ca} = 973\,440$ evolutions. $N_{pop}^{EPSDE} = 20$, $G_{en}^{EPSDE} = 200$

n.	κ_M	κ_S	ΣI_{UL}	<i>FAR</i> %	ΣG_{OL}	<i>FRR</i> %	<i>ERR</i> % / pixel	Tot. time
1	1	1	3742	3.49	36	3.46	3.49 / 2902	1.970
2	1	5	3802	3.54	39	3.75	3.54 / 576	0.480
3	1	10	3917	3.65	42	4.03	3.65 / 268	0.290
4	1	15	4117	3.84	47	4.51	3.84 / 232	0.220
5	1	20	4627	3.31	50	4.80	3.31 / 201	0.190
6	1	25	4790	4.47	53	5.09	4.47 / 170	0.160
7	1	30	5237	4.88	57	5.48	4.88 / 120	0.140
8	1	35	5701	5.32	59	5.67	5.32 / 101	0.140
9	1	40	5744	5.36	59	5.67	5.36 / 82	0.140

area between fingers – in root of fingers. This effect was observed without regard to type of used contour M_{co}, M_{ea}, S_{ea} . It is the reason why use of only rule R_I does not lead to such good results in comparison to use of combination $R_H + R_I$. Thanks to rule R_H the ICP algorithm correctly matches contours M and S . In the course of experiments the value κ_S was changed in range $\kappa_S = 1 - 40$ for whole time of evolution in accordance to Tab. 7. The reason of test of various values κ_S is of course, in an effort to ascertain how much the

estimator **eaICP** is robust/stable at a lower number of points which make the hand contour. For $\kappa_S = 40$ e.g. A1: values $FAR = 0.63\%$, $FRR = 0.67\%$, $EER = 0.63\%$ was reached - see Tab. 8. For all other assemblages the results are worse. Proposed **eaICP** estimator in assemblage A1 is very robust and offers very good results. In Fig. 15 curves FAR, FRR for results in Tab. 2 are displayed. In Fig. 16 are displayed corresponding ROC (Receive Operating Characteristics) curves for individual tested values κ_S in range $\kappa_S = 1 - 40$.

Table 8

Statistics of success rate of estimator A7, values FAR, FRR, EER , see Tab. 1. A7: THID, 640x480, $C_{1-8}^{M_{co}}, C_{1-8}^{S_{ea}}$, 5 fingers, $R_H + R_I$, $P_{\kappa_1-6}, D_m = 9, E8$. Time demands in [sec.ms] are assumed for successful alignment of samples THID: **P001-03-M** a **P057-08-S** – samples see Fig. 12. Total number of evolutions is: 9 rows \times 108160 comparisons M_{co} vs $S_{ea} = 973\,440$ evolutions. $N_{pop}^{EPSDE} = 20, G_{en}^{EPSDE} = 200$

n.	κ_M	κ_S	ΣI_{UL}	$FAR\%$	ΣG_{OL}	$FRR\%$	$ERR\% / \text{pixel}$	Tot. time
1	1	1	1956	1.82	19	1.82	1.82 / 2199	2.496
2	1	5	1960	1.82	19	1.82	1.82 / 435	0.608
3	1	10	1958	1.82	19	1.82	1.82 / 215	0.343
4	1	15	1970	1.83	20	1.92	1.84 / 198	0.280
5	1	20	1982	1.85	19	1.82	1.85 / 140	0.218
6	1	25	1989	1.85	20	1.92	1.85 / 100	0.202
7	1	30	1998	1.86	20	1.92	1.86 / 74	0.187
8	1	35	2008	1.87	20	1.92	1.87 / 56	0.171
9	1	40	2010	1.87	20	1.91	1.87 / 49	0.156

For experiments with GPDS database (94 persons - genuine \times 940 images impostors + genuine, 10 images of every person, totally 88360 comparisons) an assemblage of estimators named A8-A11 were elected – see Tab. 1 and Tab. 9-12, 13 with different image resolution, number of fingers and contours. The best result was reached for assemblage A8: $FAR = 0.35\%$, $FRR = 0.31\%$, $EER = 0.35\%$, $IR = 99.68\%$ for native image resolution 1403x1021 pixels – see Tab. 9 and Fig. 17. In Fig. 17 ROC curves are recorded for individual rows in Tab. 9, assemblage A8. In several cases it was not possible to classify a contour because one of images obtained from an identical person had e.g. shorter fingers or the fingers were unexpectedly deformed e.g. shorter of 10mm etc. – see Fig. 18. Unfortunately,

the **eaICP** estimator is very sensitive to such similar anomalies. In paper [4] authors reached, with use of identical database, values $FAR = 1.50\%$, $FRR = 3.50\%$ for database of size 50 persons and results values $FAR = 1.50\%$, $FRR = 5.95\%$ for database of size 100 persons. In paper [5] authors attained values $FAR = 0.50\%$, $FRR = 2.00\%$ for 100 persons in database GPDS. In Tab. 9, assemblage A8, row 8 a value $EER = 0.26\%$ is recorded for $\kappa_S = 35$. The processed task and whole **eaICP** mechanism represents a strongly non-linear system. The calculation was repeated several times with identical result (or almost identical) and it was ascertained that this phenomenon is only “a piece of luck”. For image resolution 640x480 pixels - see Tab. 10-128, **eaICP** estimator attained values A9: $FAR = 0.63\%$,

Table 9

Statistics of success rate of estimator A8, values FAR , FRR , EER , see Tab. 1. A8: GPDS, 1403x1021, $c_{4-8}^{M_{co}}$, $c_{4-8}^{S_{ea}}$, 4 fingers, $R_H + R_I$, R_{K3-6} , $D_{im} = 7$, E9. Time demands in [sec.ms] are assumed for successful alignment of samples **GPDS: P001-03-M a P057-08-S**. Total number of evolutions is: 9 rows \times 88360 comparisons M_{co} vs $S_{ea} = 795\,240$ evolutions. For row 1 is the value Identification Rate (IR) equal to 99.68%. $N_{pop}^{EPSDE} = 40$, $G_{en}^{EPSDE} = 420$

n.	κ_M	κ_S	ΣI_{UL}	$FAR\%$	ΣG_{OL}	$FRR\%$	$ERR\% / \text{pixel}$	Tot. time
1	1	1	310	0.35	3	0.31	0.35 / 6006	42.470
2	1	5	311	0.35	3	0.31	0.35 / 1190	10.400
3	1	10	331	0.36	3	0.28	0.37 / 593	5.220
4	1	15	413	0.38	4	0.38	0.42 / 400	3.580
5	1	20	370	0.42	4	0.42	0.42 / 297	2.680
6	1	25	276	0.36	3	0.31	0.36 / 230	2.270
7	1	30	333	0.38	4	0.42	0.38 / 193	1.900
8	1	35	229	0.26	3	0.31	0.26 / 160	1.650
9	1	40	368	0.42	4	0.42	0.42 / 147	1.550

Table 10

Statistics of success rate of estimator A9, values FAR , FRR , EER , see Tab. 1. A9: GPDS, 640x480, $c_{1-8}^{M_{co}}$, $c_{1-8}^{S_{ea}}$, 5 fingers, R_I , R_{K1-6} , $D_{im} = 9$, E3. Time demands in [sec.ms] are assumed for successful alignment of samples **GPDS: P001-03-M a P057-08-S**. Total number of evolutions is: 9 rows \times 88360 comparisons M_{co} vs $S_{ea} = 795\,240$ evolutions. $N_{pop}^{EPSDE} = 20$, $G_{en}^{EPSDE} = 200$

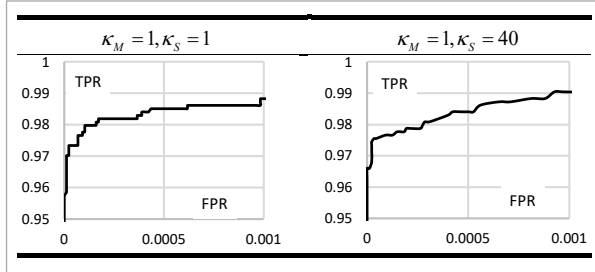
n.	κ_M	κ_S	ΣI_{UL}	$FAR\%$	ΣG_{OL}	$FRR\%$	$ERR\% / \text{pixel}$	Tot. time
1	1	1	559	0.63	6	0.63	0.63 / 2455	4.210
2	1	5	1216	1.39	13	1.38	1.39 / 533	0.970
3	1	10	1232	1.40	13	1.39	1.40 / 250	0.630
4	1	15	1255	1.43	14	1.43	1.41 / 212	0.450
5	1	20	1274	1.45	14	1.45	1.44 / 189	0.380
6	1	25	1285	1.46	14	1.48	1.46 / 115	0.310
7	1	30	1623	1.85	17	1.80	1.85 / 87	0.270
8	1	35	1625	1.85	18	1.91	1.85 / 87	0.260
9	1	40	1640	1.87	18	1.91	1.87 / 76	0.255

$FRR = 0.63\%$, $EER = 0.63\%$ and for A10: $FAR = 2.12\%$, $FRR = 2.12\%$, $EER = 2.12\%$. A worse result for A10 in comparison to A9 is given thanks to a thumb that has only one knuckle, while the second knuckle is strongly fixed. Identical results were reached for THID database too. In both the cases A9 and A10 only one classification criteria R_I was used, without some heuristic rules. For assemblage A11, Tab. 12 were recorded values $FAR = 0.64\%$, $FRR = 0.63\%$, $EER = 0.64\%$. In compar-

ison of results for A8 and A11 it is well visible that decrease of image resolution has significant effect on final accuracy. Values for A11 are fifty percent worse than for A8 at preservation of all other working parameters (except resolution). A difference between A9, A10 and A11 is that A11 compares two contours of type M_{co} , S_{ea} . The A9, A10 compares contours M_{ea} , S_{ea} . According to attained results it is highly visible that the final result is highly effected in the case of comparison of 5-fin-

Figure 17

Selected ROC curves for estimator A8 in Tab. 9. A8: GPDS, 1403x1021, $c_{4-8}^{M_{co}}$, $c_{4-8}^{S_{ca}}$, 4 fingers, $R_H + R_I$, R_{K3-6} , $D_{im} = 7$, E9. Horizontal axis–False Positive Rate (FPR), Vertical axis–True Positive Rate (TPR)



gered contour with two knuckles of the thumb. This effect is also given by high quality images in the GPDS database. This is more superior in comparison to the THID database. From results in Tabs. 9-12 it follows that proposed estimators are markedly robust. For assemblage A8 and A11 the reached EER results are nearly invariable even for the coefficient $\kappa_S = 40$. For assemblage A11 – GPDS database, this means that ICP algorithm matches contours with only approx. 10 points for every one of 4 fingers. In paper [56] also used the GPDS database with the number of persons being 100. Unfortunately, authors did not report values for FAR, FRR, EER , but for GPDS database they

Table 11

Statistics of success rate of estimator A10, values FAR, FRR, EER , viz Tab. 1, A10: GPDS, 640x480, $c_{1-8}^{M_{co}}$, $c_{1-8}^{S_{ca}}$, 5 fingers, R_I , R_{K1-6} , R_{K2} fixed, $D_{im} = 8$, E11. Time demands in [sec.ms] are assumed for successful alignment of samples **GPDS: P001-03-M** a **P057-08-S**. Total number of evolutions is: 9 rows \times 88360 comparisons M_{ea} vs $S_{ca} = 795\,240$ evolutions. $N_{pop}^{EPSDE} = 20$, $G_{en}^{EPSDE} = 200$

n.	κ_M	κ_S	ΣI_{UL}	$FAR\%$	ΣG_{OL}	$FRR\%$	$ERR\% / \text{pixel}$	Tot. time
1	1	1	1856	2.12	20	2.12%	2.12 / 3324	4.290
2	1	5	1876	2.14	20	2.12%	2.14 / 676	0.990
3	1	10	1894	2.16	21	2.23%	2.16 / 345	0.520
4	1	15	2169	2.48	23	2.44%	2.48 / 239	0.420
5	1	20	1967	2.25	22	2.34%	2.25 / 181	0.350
6	1	25	2218	2.53	25	2.65%	2.53 / 150	0.300
7	1	30	2304	2.63	23	2.44%	2.63 / 127	0.270
8	1	35	2405	2.75	26	2.76%	2.75 / 113	0.250
9	1	40	2613	2.98	28	2.97%	2.98 / 100	0.200

Table 12

Statistics of success rate of estimator A11, values FAR, FRR, EER , viz Tab. 1, A11: GPDS, 640x480, $c_{4-8}^{M_{co}}$, $c_{4-8}^{S_{ca}}$, 4 fingers, $R_H + R_I$, R_{K3-6} , $D_{im} = 7$, E9. Time demands in [sec.ms] are assumed for successful alignment of samples **GPDS: P001-03-M** a **P057-08-S**. Total number of evolutions is: 9 rows \times 88360 comparisons M_{co} vs $S_{ca} = 795\,240$ evolutions. $N_{pop}^{EPSDE} = 20$, $G_{en}^{EPSDE} = 200$

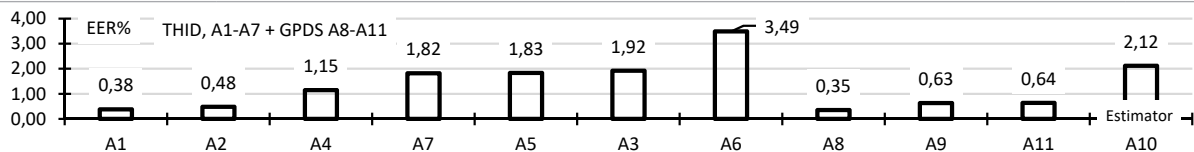
n.	κ_M	κ_S	ΣI_{UL}	$FAR\%$	ΣG_{OL}	$FRR\%$	$ERR\% / \text{pixel}$	Tot. time
1	1	1	561	0.64	6	0.63	0.64 / 1371	3.280
2	1	5	561	0.64	6	0.64	0.64 / 268	0.840
3	1	10	560	0.64	6	0.64	0.64 / 136	0.500
4	1	15	560	0.64	6	0.64	0.64 / 115	0.360
5	1	20	561	0.64	6	0.64	0.64 / 97	0.300
6	1	25	560	0.64	6	0.63	0.64 / 85	0.250
7	1	30	561	0.64	6	0.63	0.64 / 67	0.240
8	1	35	561	0.64	6	0.64	0.64 / 46	0.210
9	1	40	560	0.64	6	0.63	0.64 / 29	0.200

Table 13

Comparison of efficiency of the **eaICP** with other works with use of statistical coefficient EER

n.	Author	Method, database, success rate	EER%
1	[56]	DHMMK + SVM, GPDS db. + UST db., GPDS db. succ. rate 99.87%, 3 templates UST db. succ. rate 100%, 99.2%	0.31
2	[55]	SVM, 5 fingers, GPDS db., succ. rate 99.9%	-
3	[14]	Hand geometry + palmprint, 4 fingers, proprietary db., DCT: GAR=99.5%	1.1198
4	[50]	Shape + Geom., IITD db., EER=0.52%, Shape + Geom., propriet. db., EER=0.31%	0.52, 0.31
5	[31]	2D+3D Hand geometry, proprietary db.	0.22
6	[31]	2D Hand geometry, proprietary db.	6.3
7	[21]	Geometry + palm texture, proprietary db.	0.17
8	[48]	SVM, k-NN, HTC db., UST db., IIT db.	2.5,2,0,14
9	[49]	Contour, parametric curve, proprietary db.	3.7
10	[30]	Fourier descriptors, 4 fingers, Bogazici University Hand Database	3.69, 2.73
11	[35]	GPDS db., CASIA db., IITD-TPD db., Casia, GA-LDA: EER=4.64%, IITD, GA-LDA: EER=4.51%	4.51, 4.61
12	[38]	SVM, 3 fingers, proprietary db.	3.4
13	[9]	k-NN, RF classifier, 4 fingers, 5 fingers, Bogazici University Hand Database	6.0, 8.0
14	[16]	ICA, left + right hand, palmprint, shape + texture fusion, proprietary db.	1.0, 0.33
15	[63]	Hand shape, ICA, 5 fingers, proprietary db. 458 persons, c. 99.48% succ. rate	6.14
16	[34]	Hand geometry, proprietary db., FAR=5.29%, FRR=8.34%	-
17	[4]	Geometry + SVM, GPDS db., FAR=1.5%, FRR=3.5%	-
18	[5]	Geometry, 16 topologies of minimal edge connected graph, Euklid. dist., GPDS db., 50 persons: FAR=0.0%, FRR=1.5%, 100 persons: FAR=0.5%, FRR=2.0%	-
19	[33]	Set of features, abs. value from difference of features + weight coefs., 4 fingers, HGDB, FAR=0.00%, FRR=1.19%	0.59
20	[8]	Euclidean distance, THID db.	3.5
21	[8]	LDA, hand geometry + subset selection with Decidability, THID db.	0.9
22	[8]	Hand geom., subset sel. with intra/inter-class variability, LDA, 4 fingers, THID db.	0.52
23	This work, A1	Geometry+topology, 4 fingers, M_{co}, S_{ea}, THID db., 1280x960, IR%=100, E9	0.38
24	This work, A2	Geometry+topology, 4 fingers, 4 knuckles, M_{co}, S_{ea} , THID db., 1280x960, E9	0.48
25	This work, A3	Geometry, 4 fingers, 4 knuckles, M_{co}, S_{ea} , THID db., 1280x960, E5	1.92
26	This work, A4	Geometry+topology, 4 fingers, 4 knuckles, M_{co}, S_{ea} , THID db., 640x480, E9	1.15
27	This work, A5	Geometry+topology, 4 fingers, 4 knuckles, M_{co}, S_{ea} , THID db., 640x480, E10	1.83
28	This work, A6	Geometry, 4 fingers, 5 fingers, 5 knuckles, M_{co}, S_{ea} , THID db., 640x480, E11	3.49
29	This work, A7	Geometry+topology, 5 fingers, 6 knuckles, M_{co}, S_{ea} , THID db., 640x480, E8	1.82
30	This work, A8	Geometry+topology, 4 fingers, M_{co}, S_{ea}, GPDS db., 1403x1021, E9	0.35
31	This work, A9	Geometry, 5 fingers, 6 knuckles, M_{co}, S_{ea} , GPDS db., 640x480, E3	0.63
32	This work, A10	Geometry, 5 fingers, 5 knuckles, M_{co}, S_{ea} , GPDS db., 640x480, E11	2.12
33	This work, A11	Geometry+topology, 5 fingers, 4 knuckles, M_{co}, S_{ea} , GPDS db., 640x480, E9	0.64

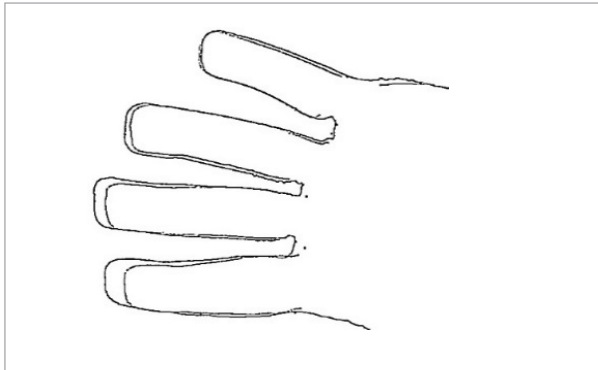
Order of estimators A1-A7 (THID), A8-A11 (GPDS) according to efficiency expressed by EER coefficient in percent.



reached values of $IR = 99.87\%$ for comparative template assembled with three contours of an identical person. For the template assembled with only one image of an identical person $IR = 99.42\%$.

Figure 18

Different length of fingers for identical person on different images. Difference is up to 1cm. A difference is also in thickness and shape of some of the 5 fingers from an identical person. The reason is that the scanned person put his hand on the pad in bad manner



5. Discussion

When in 1996 [44] presented the DE algorithm, all looked very hopeful. The optimizer was created which relatively easily could optimize a large number of tasks. Sadly, year after year it was proved true that DE is very hard to use thanks to a large number of working parameters, which it is necessary to change running time of the optimizer see e.g. [17] etc. DE is a very powerful instrument for optimization of some low-dimensional tasks e.g. in areas of robotics – laser navigation of cars [39, 40] with use of 2D laser, which is 2 or 3-dimensional task. This task solves so called continual localization. At increasing number of dimensions of an optimization task solved using DE, negative features arise originating from incapability of automatic change of working parameters of the original DE - and it is necessary to use some more advanced optimizer.

Evolutionary algorithms are not only one means, with which is possible to solve certain groups of optimization tasks. There is an uncountable number of ways. E.g. [8] presented the method for person identification which uses the Linear Discriminant Analysis (LDA) algorithm. An identical approach can be also

found in [35]. The main disadvantage of the LDA is its complexity $O(M^3)$ or in the best case $O(NM^2)$. The whole system proposed by [8] is relatively complicated in itself and its practical realization requires cooperation of more workers. This rule holds also for other commonly used methods such as SVM (Support Vector Machines), k-NN (k-nearest-neighborhood) see [35]. If it is necessary to create everything from scratch this is a relatively short time-period. Evolutionary algorithm usually makes another, higher level, superior level for already existing methods. Thanks to that, the whole algorithm development process is many times more complicated. However, thanks to evolutionary algorithms it is possible to cut-down computational demands, sometimes radically. The most important thing is that resulting accuracy stays identical or can be even better see „**eaICP** vs [8]“. Something similar can not be reached without the use of evolutionary algorithms. An absolutely typical example is described in a couple of methods [6] vs. [41]. For presented **eaICP** estimator it is possible, thanks to used evolutionary optimizers, to cut down computational complexity to value $O(N)$, where for the value N there is strongly fixed maximal limit with regard to physiological features of a human. The disadvantage of using evolutionary algorithms is that practical realization requires “an intelligent” approach and experiences. The theorem [61] which says that “nothing is free” holds, sadly, for evolutionary algorithms twice.

6. Conclusion

In the presented paper the proposed algorithm, marked as **eaICP**, enables identification of a person with use of knowledge of human hand contours and their complexity is $O(N)$. The best reached accuracy is expressed by the EER coefficient for individual tested databases THID: EER=0.38%, GPDS: EER=0.35%. It was proven that significant influence on final accuracy was the quality of model contour and the number of points (entities in general sense), from which the contour is assembled. The whole process of classification strongly depends on modern technologies and also on the computational potential of commonly reasonable priced processors. During contour classification many findings were used from many branches of artificial intelligence which at the same time mirrors the state-of-

the-art in the affected areas. The aim of this study was to find if it is possible to successfully solve the given 7, 8 and 9-dimensional task with use of modern evolutionary optimizers. The group of suitable optimizers was found. The **eaICP** algorithm uses the most up-to-date classification methods which are commonly used in many sensitive medical and military areas.

Acknowledgment

I would like to express my cordial thanks to Prof. Janez Demšar for his help with Demšar significance diagram and Friedman-posthoc Nemnyi-Demšar systematics, to Charles Zaiontz, Ph.D. for his help with

Friedman-Cochran-posthocNemnyi systematics and to Jaroslav Marek, Ph.D. for his advice of ANOVA statistics and pivot tables.

Author would like to express cordial thanks to Mr. Paul Hooper for his careful English text correction, patience and stamina.

I would like to express my cordial thanks to “Microsoft Azure” virtual computer which helped to compute Table 9, row 1, estimator A8 result thanks to free 200USD credit for everyone.

The publication was supported by the funds of University of Pardubice, Czech Republic – Student grant competition project (SGS_2019_021).

References

- Abaza, A., Ross, A., Hebert, Ch., Harrison, M. A., Nixon, M. S. A Survey on Ear Biometric. *Journal ACM Computing Surveys*, 2013, 45(22), 35. <https://doi.org/10.1145/2431211.2431221>
- Abbass, A. H. The Self-Adaptive Pareto Differential Evolution Algorithm. *Proceedings of the 2002 Congress on Evolutionary Computation*, 2002, 1, 831-836.
- Alani, H. A. Enhanced Geometric - Based Hand Recognition Using Neural Network. *International Journal of Scientific & Engineering Research*, 2014, 5(6), 168-171.
- Angadi, S. A., Hatture, M. S. Biometric Person Identification System: A Multimodal Approach Employing Spectral Graph Characteristics of Hand Geometry and Palmprint, *Intelligent Systems and Applications*, 2016, 3, 48-58, DOI: 10.5815/ijisa.2016.03.06. <https://doi.org/10.5815/ijisa.2016.03.06>
- Angadi, S. A., Hatture, M. S. Hand Geometry-Based User Identification Using Minimal Edge Connected Hand Image Graph. *IET Computer Vision*, 2018, 12(5), 744-752. <https://doi.org/10.1049/iet-cvi.2017.0053>
- Asari, K. V., Kumar, S., Radhakrishnan, D. A New Approach for Nonlinear Distortion Correction In Endoscopic Images Based on Least Squares Estimation. *IEEE Transaction on Medical Imaging*, 1999, 18(4), 345-354. <https://doi.org/10.1109/42.768843>
- Bakshe, R. C., Patil, A. M. Hand Geometry Techniques: A Review. *International Journal of Modern Communication Technologies & Research*, 2014, 2(11), 7.
- Barra, S., Marsico, M., Nappi, M., Narducci, F., Riccio, D. A Hand-Based Biometric System. *Visible Mobile Environments, Information Sciences*, 2019, 479, 472-485. <https://doi.org/10.1016/j.ins.2018.01.010>
- Bera, A., Bhattacharjee, D. Human Identification Using Selected Features From Finger Geometric Profiles, *IEEE Transactions on System, Man and Cybernetics: Systems*, 2017, 1-15.
- Besl, P. J., McKay, H. D. A Method for Registration of 3-D Shapes. *IEEE Transaction on Pattern Analysis and Machine Intelligence*, 1992, 14(2), 239-256. <https://doi.org/10.1109/34.121791>
- Brest, J., Greiner, S., Boškovič, B., Mernik, M., Žumer, V. Self-adapting Control Parameters in Differential Evolution: A Comparative Study on Numerical Benchmark Problems. *IEEE Transactions on Evolutionary Computation*, 2006, 10(6), 646-657. <https://doi.org/10.1109/TEVC.2006.872133>
- Charette, R. Looking at Your Ears: The New Biometric Security Scan? *IEEE Spectrum Journal*, 2010.
- Dai, D. Q., Yuen, P. C. Regularized Discriminant Analysis and Its Application to Face Recognition, *Pattern Recognition*, 2003, 36(3), 845-847. [https://doi.org/10.1016/S0031-3203\(02\)00092-4](https://doi.org/10.1016/S0031-3203(02)00092-4)
- Dale, M. P., Joshi, M. A., Galiyawala, H. J. A Single Sensor Hand Geometry and Palm Texture Fusion for Person Identification. *International Journal of Computer Applications*, 2012, 42(7), 11-16. <https://doi.org/10.5120/5703-7726>
- Duta, N. A Survey of Biometric Technology Based on Hand Shape. *Pattern Recognition*, 2009, 42, 2797-2806. <https://doi.org/10.1016/j.patcog.2009.02.007>
- Dutagaci, H., Sankur, B., Yoruk, E. Comparative Analysis of Global Hand Appearance-Based Person Recognition. *Journal of Electronic Imaging*, 2008, 17(1), 1-19. <https://doi.org/10.1117/1.2890986>

17. Eiben, A. E., Hinterding, R., Michalewicz, Z. Parameter Control in Evolutionary Algorithms. *IEEE Transaction on Evolutionary Computation*, 1999, 3(2), 124-141. <https://doi.org/10.1109/4235.771166>
18. Farnia, P., Ahmadian, A., Behnam, H., Dadashi, N. Performance Evaluation of the Modified Iterative Closest Point Methods for Intra-operative Ultrasound and Pre-operative MR Image Registration of Brain. *Frontiers in Biomedical Technologies*, 2014, 1(2), 123-131.
19. Faundez-Zanuy, M., Elizondo, D. A., Ferrer-Ballester M. A., Travieso-González, C. M. Authentication of Individuals Using Hand Geometry Biometrics: A Neural Network Approach. *Neural Processing Letters*, 2016, 26, 201-216. <https://doi.org/10.1007/s11063-007-9052-y>
20. Faundez-Zanuy, M., Mekyska, J., Font-Aragones, X. A New Hand Image Database Simultaneously Acquired in Visible, Near-Infrared and Thermal Spectrums. *Cognitive Computation*, 2014, 6(2), 230-240. <https://doi.org/10.1007/s12559-013-9230-3>
21. Ferrer, M. A., Morales, A., Travieso, C. M., Alonso, J. B. Low Cost Multimodal Biometric Identification System Based on Hand Geometry, Palm and Finger Textures. *41st Annual IEEE International Carnahan Conference on Security Technology*, 2007, 52-58. <https://doi.org/10.1109/CCST.2007.4373467>
22. Ferrer, M. A., Vargas, F., Morales, A. Bi-Spectral Contactless Hand Based Biometric Identification Device. *2nd National Conference on Telecom*, 2011, 267-284. DOI: 10.5772/18096. <https://doi.org/10.5772/18096>
23. Font-Aragones, X., Faundez-Zanuy, M., Mekyska, J. Thermal Hand Image Segmentation for Biometric Recognition. *IEEE Aerospace and Electronic Systems Magazine*, 2013, 28(6), 4-14. <https://doi.org/10.1109/MAES.2013.6533739>
24. Hansen, N., Ostermeier, A. Adapting Arbitrary Normal Mutation Distributions in Evolution Strategies: The Covariance Matrix Adaptation. *IEEE International Conference on Evolutionary Computation*, 1996, 312-317.
25. Hansen, N., Ostermeier, A. Completely Derandomized Self-Adaptation in Evolution Strategies. *Evolutionary Computation*, 2001, 9(2), 159-195. <https://doi.org/10.1162/106365601750190398>
26. Hansen, N., Ostermeier, A. Convergence Properties of Evolution Strategies with the Derandomized Covariance Matrix Adaptation: The $(\mu/\mu I, \lambda)$ -ES. *EUFIT'97, 5th European Congress on Intelligent Techniques and Soft Computing*, 1997, 650-654.
27. Holland, J. H. *Adaptation in Natural and Artificial Systems*, University of Michigan Press, Ann Arbor, 1975.
28. Holland, J. H. *Adaptation in Natural and Artificial Systems: An Introductory Analysis with Application to Biology, Control, and Artificial Intelligence*, Cambridge, MIT Press, 1992. <https://doi.org/10.7551/mitpress/1090.001.0001>
29. Jain, A. K., Ross, A., Prabhakar, S. An Introduction to Biometric Recognition. *IEEE Transactions on Circuits and Systems for Video Technology*, 2000, 14(1), 4-20. <https://doi.org/10.1109/TCSVT.2003.818349>
30. Kang, W., Wu, Q. Pose-invariant Hand Shape Recognition Based on Finger Geometry. *IEEE Transactions on System Man and Cybernetics Systems*, 2014, 44(11), 1510-1521. <https://doi.org/10.1109/TSMC.2014.2330551>
31. Kanhangad, V., Kumar, A., Zhang, D. Combining 2D and 3D Hand Geometry Features for Biometric Verification. *IEEE Computer Society Conference on Computer Vision and Pattern Recognition Workshops*, 2009. <https://doi.org/10.1109/CVPRW.2009.5204306>
32. Kennedy, J., Eberhart, R. C. Particle Swarm Optimization. *IEEE International Conference on Neural Networks*, 1995, 4, 1942-1948.
33. Klonowski, M., Plata, M., Syga, P. User Authorization Based on Hand Geometry Without Special Equipment. *Pattern Recognition*, 2018, 73, 189-201. <https://doi.org/10.1016/j.patcog.2017.08.017>
34. Kumar, A., Wong, D. C. M., Shen, H. C., Jain, A. K. Personal Verification Using Palmprint and Hand Geometry Biometric. *International Conference on Audio and Video Based Biometric Person Authentication*, 2003, 668-678. https://doi.org/10.1007/3-540-44887-X_78
35. Luque-Baena, R. M., Elizondo, D., López-Rubio, E., Palomo, E. J., Watson, T. Assessment of Geometric Features for Individual Identification and Verification in Biometric Hand Systems. *Expert Systems and Applications*, 2013, 40(9), 3580-3594. <https://doi.org/10.1016/j.eswa.2012.12.065>
36. Maier-Hein, L., Franz, A. M., Santos, T. R., Schmidt, M., Fangerau, M., Meinzer, H. P., Fitzpatrick, J. M. Convergent Iterative Closest-point Algorithm to Accommodate Anisotropic and Inhomogenous Localization Error. *IEEE Transactions on Pattern Analysis and Machine Intelligence*, 2012, 34(8), 1520-1532. <https://doi.org/10.1109/TPAMI.2011.248>
37. Mallipeddi, R., Suganthan, P. N. Differential Evolution Algorithm with Ensemble of Parameters and Mutation and Crossover Strategies. *International Conference on Swarm, Evolutionary, and Memetic Computing SEMCCO 2010*, 2010, 71-78. https://doi.org/10.1007/978-3-642-17563-3_9
38. Morales, A., Ferrer, M. A., Díaz, F., Alonso J. B., Travieso C. M. Contact-Free Hand Biometric System for Real Environments. *16th European Signal Processing Conference*, 2008. <https://doi.org/10.5772/7447>

39. Moravec, J., Hub, M. Camera Calibration Using Direct Mapping and Adaptive Metaheuristic. *International Journal of BioScience and BioTechnology*, 2015, 7(3), 111-120. <https://doi.org/10.14257/ijbsbt.2015.7.3.11>
40. Moravec, J., Pošík, P. A Comparative Study: The Effect of the Perturbation Vector Type in the Differential Evolution Algorithm on the Accuracy of Robot Pose and Heading Estimation. *Evolutionary Intelligence Journal*, 2014a, 6(3), 171-191. <https://doi.org/10.1007/s12065-013-0090-2>
41. Moravec, J., Pošík, P. Global Robot Localization Under Noise Stress Utilizing EA Methods and Semi-semantic Classification of a Known Environment. *Applied Artificial Intelligence*, 2014b, 28(4), 360-417. <https://doi.org/10.1080/08839514.2014.875684>
42. Polap, D., Wozniak, M. Polar Bear Optimization Algorithm: Meta-Heuristic with Fast Population Movement and Dynamic Birth and Death Mechanism. *Symmetry*, 2017, 1-20. <https://doi.org/10.3390/sym9100203>
43. Pottmann, H., Huang, Q. X., Yang Y. L., Hu, S. M. Geometry and Convergence Analysis of Algorithms for Registration of 3D Shapes. *International Journal on Computer Vision*, 2006, 67(3), 277-296. <https://doi.org/10.1007/s11263-006-5167-2>
44. Price, K. Differential Evolution: A Fast and Simple Numerical Optimizer. *NAFIPS'96*, 1996, 524-527.
45. Qin, A. K., Suganthan, P. N. Self-adaptive Differential Evolution Algorithm for Numerical Optimization. *IEEE Congress on Evolutionary Computation*, 2005, 2, 1785-1791.
46. Rodrigues, M., Fisher, R., Liu, Y. Special Issue on Registration and Fusion of Range Images. *Computer Vision and Image Understanding*, 2002, 87, 1-131. <https://doi.org/10.1006/cviu.2002.0978>
47. Sanches-Reillo, S. R., Sanches-Avila, S. C., Gonzales-Marcos, A. Biometric Identification Through Hand Geometry Measurement. *IEEE Transactions on Pattern Analysis and Machine Intelligence*, 2000, 22(10), 1168-1171. <https://doi.org/10.1109/34.879796>
48. Santos-Sierra, A., Casanova, J., Avila, C., Vera, V. Silhouette-Based Hand Recognition on Mobile Devices. *International Carnahan Conference on Security Technology*, 2009, 160-166. <https://doi.org/10.1109/CCST.2009.5335548>
49. Santos-Sierra, A., Sánchez-Ávila, C., Pozo, G. B., Guerra-Casanova, J. Unconstrained and Contactless Hand Geometry Biometrics. *Sensors*, 2011, 11, 10143-10164. <https://doi.org/10.3390/s111110143>
50. Sharma, S., Dubey, S. R., Singh, S. K., Saxena, R., Singh R. K. Identity Verification Using Shape and Geometry of Human Hands. *Expert Systems and Applications*, 2015, 42(2), 821-832. <https://doi.org/10.1016/j.eswa.2014.08.052>
51. Smit, S. K., Eiben, A. E. Comparing Parameter Tuning Methods for Evolutionary Algorithms. *IEEE Congress on Evolutionary Computation*, 2009, 399-406. <https://doi.org/10.1109/CEC.2009.4982974>
52. Smit, S. K., Eiben, A. E. Parameter Tuning for Configuring and Analyzing Evolutionary Algorithms. *Swarm and Evolutionary Computation*, 2010a, 1(1), 19-31. <https://doi.org/10.1016/j.swevo.2011.02.001>
53. Smit, S. K., Eiben, A. E. Parameter Tuning of Evolutionary Algorithms: Generalist vs. Specialist. *Applications of Evolutionary Computation*, 2010b, 6024, 542-551. https://doi.org/10.1007/978-3-642-12239-2_56
54. Teo, J. Exploring Dynamic Self-Adaptive Populations in Differential Evolution. *Soft Computing*, 2006, 10, 673-686. DOI 10.1007/s00500-005-0537-1. <https://doi.org/10.1007/s00500-005-0537-1>
55. Travieso, C. M., Alonso, J. B., David, S., Ferrer, M. A. Optimization of a Biometric System Identification by Hand Geometry. *Complex Systems Intelligence and Modern Technological Applications*, Cherbourg, France, 2004, 581-586.
56. Travieso, C. M., Briceo, J. C., Alonso, J. B. Transformation of Hand-Shape Features for a Biometric Identification Approach. *Sensors*, 2012, 12(1), 987-1001. <https://doi.org/10.3390/s120100987>
57. Urfahoglu, O. Robust Estimation of Camera Rotation, Translation and Focal Length at High Outlier Rates. *1st Canadian Conference on Computer and Robot Vision*, 2004, 464-471.
58. Web1: <http://splab.cz/en/download/database/tecnocampus-hand-image-database>, Accessed November 2019
59. Web2: <http://www.gpds.ulpgc.es/>, Accessed November 2019
60. Web3: www.handwork.4fan.cz, Accessed November 2019
61. Wolpert, D. H., Macready, W. G. No Free-Lunch Theorems for Search. *Technical Report 95-02-010*, Santa Fe Institute, 1995.
62. Yang, Z., Tang, K., Yao, X. Self-adaptive Differential Evolution with Neighborhood Search. *IEEE Congress on Evolutionary Computation*, 2008, 1110-1116.
63. Yörük, E., Konukoglu, E., Sankur, B., Darbon, J. Shape Based Hand Recognition. *IEEE Transactions on Image Processing*, 2006, 15(7), 1803-1815. <https://doi.org/10.1109/TIP.2006.873439>
64. Zhang, J., Sanderson, A. C. JADE: Adaptive Differential Evolution with Optional External Archive. *IEEE Transactions on Evolutionary Computation*, 2009, 13(5), 945-958. <https://doi.org/10.1109/TEVC.2009.2014613>